Stroke-related alterations in inter-areal communication revealed via Granger causality analysis

Michele Allegra, Chiara Favaretto, Nicholas Metcalf, Maurizio Corbetta, Andrea Brovelli

Stroke-related alterations in inter-areal communication revealed via Granger causality analysis

Michele Allegra[1], Chiara Favaretto[2,3], Nicholas Metcalf[4], Maurizio Corbetta[2,3,4]*, Andrea Brovelli[1]*

[1] Institut de Neurosciences de la Timone, Aix Marseille Université, UMR 7289 CNRS, 13005, Marseille, France

[2] Department of Neuroscience, Neurological Clinic, University of Padua, Padua, Italy

[3] Padova Neuroscience Center, University of Padua, Padua, Italy

[4] Department of Neurology, Radiology, and Neuroscience, Washington University in St. Louis, St. Louis, MO, United States

* Co-senior author

Corresponding authors:

Michele Allegra
michele.allegra@univ-amu.fr
Institut de Neurosciences de la Timone (INT),
UMR 7289 CNRS, Aix Marseille University,
Campus de Santé Timone,
27 Bd. Jean Moulin,
13385 Marseille, France

Andrea Brovelli

andrea.brovelli@univ-amu.fr

Institut de Neurosciences de la Timone (INT),

UMR 7289 CNRS, Aix Marseille University,

Campus de Santé Timone,

27 Bd. Jean Moulin,

13385 Marseille, France

Manuscript details:

Number of pages: 51

Number of figures: 8

Number of tables: 3

Number of words: 193 (abstract), 478 (introduction), 2042 (discussion), 110 (significance statement)

Abbreviations

fMRI: functional magnetic resonance imaging

FC: functional connectivity

RSNs: resting-state networks

GC: Granger causality

IC: instantaneous (Granger) causality

DC: directed (Granger) causality

UFC: undirected functional connectivity

LH/RH: left/right hemisphere

Keywords

Stroke, Granger Causality, resting state fMRI

Acknowledgements

MA, AB, CF and MC were supported by FLAG ERA II "Joint Transnational Call 2017" - HBP - Basic and Applied Research 2, Brainsynch-Hit (ANR-17-HBPR-0001) during completion of this work.

ABSTRACT

Neuroimaging and neurological studies suggest that stroke is a brain network syndrome. While causing local ischemia and cell damage at the site of injury, stroke strongly perturbs the functional organization of brain networks at large. Critically, functional connectivity abnormalities parallel both behavioral deficits and functional recovery across different cognitive domains. However, the reasons for such relations remain poorly understood. Here, we tested the hypothesis that alterations in inter-areal communication underlie stroke-related modulations in functional connectivity (FC). To this aim, we used resting-state fMRI and Granger causality analysis to quantify information transfer between brain areas and its alteration in stroke. Two main large-scale anomalies were observed in stroke patients. First, inter-hemispheric information transfer was strongly decreased with respect to healthy controls. Second, information transfer within the affected hemisphere, and from the affected to the intact hemisphere was reduced. Both anomalies were more prominent in resting-state networks related to attention and language, and they were correlated with impaired performance in several behavioral domains. Overall, our results support the hypothesis that stroke perturbs inter-areal communication within and across hemispheres, and suggest novel therapeutic approaches aimed at restoring normal information flow.

SIGNIFICANCE STATEMENT

A thorough understanding of how stroke perturbs brain function is needed to improve recovery from the severe neurological syndromes affecting stroke patients. Previous resting-state neuroimaging studies suggested that interaction between hemispheres decreases after stroke, while interaction between areas of the same hemisphere increases. Here, we used Granger causality to reconstruct information flows in the brain at rest, and analyze how stroke perturbs them. We showed that stroke causes a global reduction of inter-hemispheric communication, and an imbalance between the intact and the affected hemisphere: information flows within and from the latter are impaired. Our results may inform the design of stimulation therapies to restore the functional balance lost after stroke.

INTRODUCTION

Spontaneous brain activity is intrinsically organized into large-scale networks of correlated activity (Bullmore and Sporns, 2009; Damoiseaux et al., 2006; Fox et al., 2005), also known as resting-state networks (RSNs). The functional organization of RSNs is altered in stroke (Corbetta et al., 2018, 2015). In fact, local ischemia, which damages cells and neural connections at the site of injury, primarily affects subcortical regions and white matter, thus altering long-range functional connectivity (FC) between cortical areas. Two types of large-scale FC alterations affect RSNs (Joshua Sarfaty Siegel et al., 2016): i) a decrease of within-network interhemispheric FC (Carter et al., 2010; Golestani et al., 2013; He et al., 2007; New et al., 2015; Park Chang-hyun et al., 2011; Ramsey et al., 2016; Joshua Sarfaty Siegel et al., 2016; Tang et al., 2016); ii) an increase of between-network intra-hemispheric FC (Baldassarre et al., 2014; Eldaief et al., 2017; Ramsey et al., 2016; Joshua Sarfaty Siegel et al., 2016). As a consequence, RSNs tend to be less integrated internally, and less segregated externally, which translates into an overall decrease of network modularity (Gratton et al., 2012). The presence of such common network-level perturbations explains why lesions in different locations in the brain produce remarkably similar behavioral deficits in different patients (Corbetta et al., 2018).

The relation between FC alterations and behavioral deficits remains, however, elusive. Here, we tested the hypothesis that a key factor linking stroke-related FC modulations and behavioral deficits is the alteration in inter-areal communication. In particular, our goal was to investigate whether: i) the decrease of interhemispheric FC observed after stroke is associated with a symmetric or asymmetric decrease in information flow between areas in the damaged and non-damaged hemisphere; ii) the increase of between-network intra-hemispheric FC is paralleled by a change in intra-hemispheric information flow; iii) alterations in information flows between brains areas predict cognitive deficits across multiple domains.

To this aim, we performed covariance-based Granger Causality (GC) analyses (Brovelli et al., 2015) of resting-state fMRI data collected from stroke patients in the sub-acute phase (two weeks after stroke onset). Data were provided by the Washington university stroke database (Corbetta et al., 2015), and included structural lesions, resting-state

fMRI, and neuropsychological scores for a large cohort of first-time stroke patients and age-matched control subjects. A major advantage of covariance-based GC is the ability to analyse large networks of nodes, such as the 343 nodes used in this study, and over short time series (i.e., hundreds of data points), thus enabling direct comparison with previous FC studies. Granger causality analyses revealed that inter-hemispheric information transfer was significantly decreased in stroke patients with respect to healthy controls. In addition, a pronounced inter-hemispheric imbalance of the within-network information transfer was observed in patients. Both anomalies were more prominent in resting-state networks related to attention and language, and they paralleled deficits in several behavioral domains.

MATERIALS & METHODS

Brain imaging and behavioral measurements

Subject Enrollment and Retention. Participants (n = 172) were prospectively recruited. First-time stroke patients with clinical evidence of motor, language, attention, visual, or memory deficits based on neurological examination were included. One hundred and thirty-two patients met all inclusion criteria (for details see Corbetta et al., 2015) and completed the entire subacute protocol (mean age 52.8 years with range 22-77, 119 right-handed, 63 females, 64 right hemisphere). Patients were excluded from analysis for poor quality imaging data (n = 5), fewer than 400 frames remaining after motion scrubbing (n=8), or excessive hemodynamic lags (see below, n = 6) leaving 113 subjects in the final analysis. Demographically matched controls (n = 31) were recruited and underwent the same behavioral and imaging exams (mean age 55.7 years, SD = 11.5, range 21-83) in two separate scanning sessions (time point 1 and time point 2). Controls were matched to the study population in age, gender, handedness, and level of education. Controls were excluded based on a low number of frames after motion scrubbing (n = 4 at time point 1, n = 6 at time point 2), leaving 27 controls at time point 1 and 25 controls at time point 2.

Neuropsychological evaluation. Participants underwent a behavioral battery devised to assess motor, language, attention, memory, and visual function following each scanning session (details can be found in in Siegel et al., 2016). As described in Corbetta et al. 2015, principal components analysis was performed on all tests within a behavioral domain to produce a single score that predicted the highest percentage of variance across tasks. The left/right 'Motor' scores described left/right body motor performance that correlated across shoulder flexion, wrist extension/flexion, ankle flexion, hand dynamometer, nine-hole peg, action research arm test, timed walk, functional independence measure, and the lower extremity motricity index. The 'Visual Field Attention' score described contra-lesional attention biases in Posner, Mesulam, and behavioral inattention center-of-cancellation tasks. The 'Sustained Attention' score loaded on non-spatial measures of overall performance, reaction time, and accuracy on the same tests. The 'Shifting Attention' score loaded on tests indexing attention shifts, e.g. the difference in response times for attended *versus* unattended targets. The 'Spatial Memory' score loaded on the Brief Visuospatial Memory Test and spatial span. The 'Verbal Memory' score loaded on the Hopkins Verbal Learning Test. The 'Language' score loaded on tests devised to assess language comprehension (complex ideational material, commands, reading comprehension) and production (Boston naming, oral reading). The score of each of the seven factors for each patient was normalized using the mean and standard deviation of the corresponding factor scores in age-matched controls.

Brain imaging acquisition. Patients were scanned two weeks (mean = 13.4 days, SD=4.8 days) after stroke onset. Controls were scanned twice at an interval of 3-months. All imaging was performed using a Siemens 3T Tim-Trio scanner at the Washington University School of Medicine (WUSM) and a standard 12-channel head coil. The MRI protocol included structural, functional, pulsed arterial spin labeling (PASL), and diffusion tensor scans. Structural scans included: i) a sagittal T1-weighted MP-RAGE (TR = 1950 msec, TE = 2.26 msec, flip angle=90°, voxel size=1.0×1.0×1.0 mm); ii) a transverse T2-weighted turbo spin-echo (TR = 2500 msec, TE=435msec,

voxel- size=1.0×1.0×1.0mm); and iii) sagittal FLAIR (fluid attenuated inversion recovery) with TR = 7500 msec, TE = 326 msec and voxel-size=1.5×1.5×1.5mm. Resting-state functional scans were acquired with a gradient echo EPI sequence (TR = 2000 msec, TE = 27 msec, 32 contiguous 4 mm slices, 4×4mm in-plane resolution) during which participants were instructed to fixate a small white cross centered on a screen with a black background in a low luminance environment. Six to eight resting state fMRI runs, each including 128 volumes (for a total of 30 minutes) were acquired. A camera fixated on the eyes was used to determine when a subject's eyes were open or closed during scans. Patients had eyes open on 65.6±31.9% of frames and controls had eyes open on 76.8±30.2% of frames (t (114) = -1.7, p = 0.091).

Brain lesion masking. Lesions were manually segmented on individual structural MRI images (T1-weighted MP-RAGE, T2-weighted spin echo images, and FLAIR images obtained from 1 to 3 weeks post-stroke) using the Analyze biomedical imaging software system (www.mayo.edu; Robb and Hanson,1991). Two board-certified neurologists (Dr. Maurizio Corbetta and Dr. Alexandre Carter) reviewed all segmentations. In hemorrhagic strokes, edema was included in the lesion. A neurologist (MC) reviewed all segmentations a second time paying special attention to the borders of the lesions and degree of white matter disease. Atlas-registered segmented lesions ranged from 0.02 cm^3 to 82.97 cm^3 with a mean of 10.15 cm^3 (SD = 13.94 cm^3). Lesions were summed to display the number of patients with structural damage for each voxel.

fMRI data preprocessing. Preprocessing of fMRI data included: i) compensation for asynchronous slice acquisition using sinc interpolation; ii) elimination of odd/even slice intensity differences resulting from interleaved acquisition; iii) whole brain intensity normalization to achieve a mode value of 1000; iv) removal of distortion using synthetic field map estimation and spatial realignment within and across fMRI runs; v) resampling to 3mm cubic voxels in atlas space including realignment and atlas transformation in one resampling step. Cross-modal (e.g., T2-weighted to T1-weighted) image registration was accomplished by aligning image gradients. Cross-modal image registration in patients was checked by comparing the optimized voxel similarity

measure to the 97.5 percentile obtained in the control group. In some cases, structural images were substituted across sessions to improve the quality of registration. Following cross-modal registration, data were passed through three additional preprocessing steps. First, tissue-based regressors were computed based on FreeSurfer segmentation (Fischl, Sereno, Tootell, & Dale, 1999). The following sources of spurious variance were removed by regression: i) six parameters obtained by rigid body correction of head motion; ii) the signal averaged over the whole brain; iii) signal from ventricles and CSF; iv) signal from white matter. For Undirected Functional Connectivity (UFC) computations, we additionally regressed v) the average signal for gray matter. This step, commonly called global signal regression (GSR) was not applied for Granger causality (GC) computations. The rationale for this choice was to avoid any potential suppression of highly variable signals (Nalci et al., 2019) and distortion of information flow estimates using GC. Second, we performed temporal filtering retaining frequencies in the 0.009–0.08 Hz band. Third, we applied frame censoring meaning that the first four frames of each BOLD run were excluded. Frame censoring was implemented using frame wise displacement (Power et al., 2014) with a threshold of 1mm. This frame-censoring criterion was uniformly applied to all R-fMRI data (patients and controls).

Cortical surface processing. Surface generation and processing of functional data followed procedures similar to Glasser et al. (Glasser et al., 2013), with additional consideration for cortical segmentation in stroke patients. First, anatomical surfaces were generated for each subject's T1MRI using FreeSurfer automated segmentation (Fischl et al., 1999). This included brain extraction, segmentation, generation of white matter and pial surface, inflation of the surfaces to a sphere, and surface shape-based spherical registration to the subject's "native" surface to the fs average surface. Segmentations were manually checked for accuracy. For patients in whom the stroke disrupted automated segmentation, or registration, values within lesioned voxels were filled with normal atlas values prior to segmentation, and then masked immediately after (7 patients). The left and right hemispheres were then resampled to 164,000 vertices and registered to each other (Van Essen et al., 2001), and finally down-sampled to

10,242 vertices each (a combined total of 18,722 vertices after exclusion of the medial wall) for projection of functional data. Following preprocessing, BOLD data were sampled to each subject's individual surface (between white matter and pial surface) using a ribbon-constrained sampling available in Connectome Workbench (Marcus et al., 2013). Voxels with a high coefficient of variation (0.5 standard deviations above the mean coefficient of variation of all voxels in a 5 mm sigma Gaussian neighborhood) were excluded from volume to surface mapping (Glasser et al., 2013). Time courses were then smoothed along the 10,242 vertex surface using a 3mm FWHM Gaussian kernel. All brain surface visualizations were generated using Connectome Workbench (Marcus et al., 2013).

Brain parcellation scheme. We used a cortical surface parcellation generated by Gordon & Laumann and colleagues (Gordon et al., 2016). The parcellation is based on R-fMRI boundary mapping and achieves full cortical coverage and optimal region homogeneity. The parcellation includes 324 regions of interest (159 left hemisphere, 165 right hemisphere). Note that the original parcellation includes 333 regions, while here all regions less than 20 vertices (approximately 50 mm^2) were excluded. This cutoff was arbitrarily chosen based on the assumption that parcels below this size would have unreliable signal given 4 mm sampling of our functional data. Notably, the parcellation was generated on 120 young adults aged 18-33 and is applied here to adults aged 21-83. To generate parcel-wise connectivity matrices, time courses of all vertices within a parcel were averaged. For each ROI, we defined its center-of-mass coordinates $(\bar{x},\bar{y},\bar{z})$ as the average of the *(x,y,z)* coordinates of all vertices in the ROI. For each ROI, identified the homologous regions as the ROI in having the lowest distance from $(-\bar{x},\bar{y},\bar{z})$ (i.e., the ROI closest to be symmetrically located in the opposite hemisphere).
In addition to the 324 cortical parcels, we also defined a set of 19 sub-cortical and cerebellar regions based on the FreeSurfer segmentation: for each hemisphere 9 regions consisting of cerebellum, thalamus, caudate, putamen, pallidum, hippocampus, amygdala, accumbens and ventral dorsal caudate, plus brainstem (Fischl et al., 2002).

Granger causality analysis and inter-areal information transfer

Granger Causality (GC) framework. One of the most successful data-driven methods to quantify the degree of communication from statistical dependencies between neural signals is based on the Wiener-Granger causality principle (Granger, 1980; Brovelli et al., 2004; Ding et al., 2006; Bressler and Seth, 2011; Seth et al., 2015).

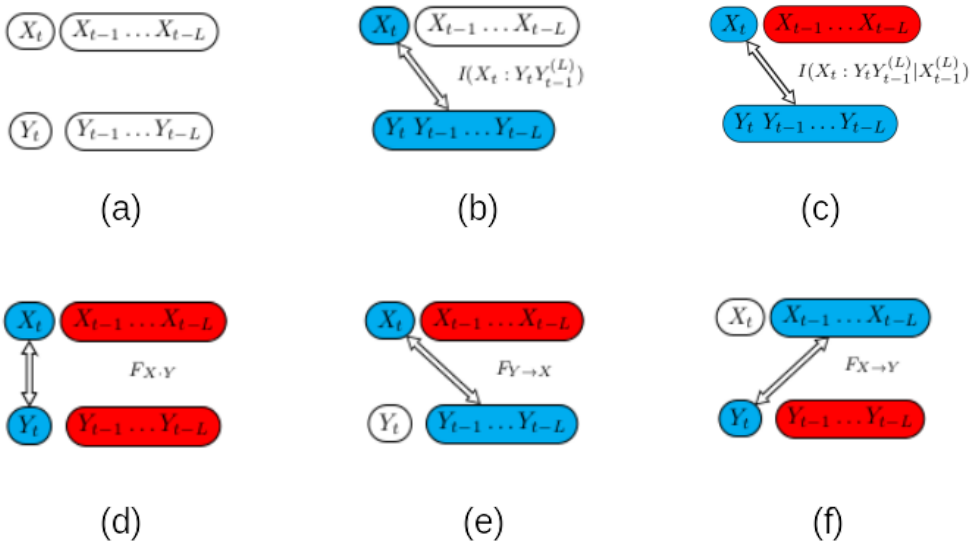

Figure 1: Dependencies between two time series. Each graph can be thought of as a representation of a conditional mutual information CMI(A:B|C) where A and B are in blue and linked by an arrow, while C is in red (a) for each time series, we consider its present value X_t and the previous *L* values in the past $X_{t-1}^{(L)} \equiv X_{t-1}, X_{t-2}, ..., X_{t-L}$. (b) The information about X_t contained in Y is defined as the MI between the present of *X* and *Y* (present and past), $I(X_t : Y_t Y_{t-1}^{(L)})$ (c) The information about X_t contained *exclusively* in Y (and not in the past values of X) is the CMI between the present of *X* and *Y* (present and past), *conditioned* on the past of X, $I(X_t : Y_t Y_{t-1}^{(L)} | X_{t-1}^{(L)})$ (d) the *instantaneous causality* measures information about X_t contained exclusively in Y_t (and not already contained in $Y_{t-1}^{(L)}$, $X_{t-1}^{(L)}$). (e) the *directed causality* from *Y* to *X* measures information about X_t contained exclusively in $Y_{t-1}^{(L)}$, (and not already contained in $X_{t-1}^{(L)}$). (f) the *directed causality* from *X* to *Y* measures information about Y_t contained exclusively in $X_{t-1}^{(L)}$, (and not already contained in $Y_{t-1}^{(L)}$).

In order to describe the Granger causality framework, let us consider two (discrete) time series $X = \{X_t\}$, $Y = \{Y_t\}$ representing the activity of two subsystems sampled at

discrete times *t={1,2,3,...,T}* within a finite time window of length *T*. Standard undirected functional connectivity (UFC) is classically computed as the Pearson's correlation, defined as $R = \frac{\sigma(X,Y)}{\sigma(X)\sigma(Y)}$ where $\sigma(X)$, $\sigma(Y)$ are the standard deviations of X_t and Y_t and $\sigma^2(X,Y)$ is their covariance within the selected time window. The UFC only considers dependencies between X_t and Y_t for the same *t*. Information-theoretically, this type of dependency is quantified by the mutual information $I(X_t : Y_t)$, which is a simple function of R for Gaussian data, $I(X_t : Y_t) = -1/2 log(1-R^2)$. The UFC is insensitive to the temporal structure of correlation between *X* and *Y*, since it is invariant under permutation of *t*. On the other hand, the framework based on Granger causality (Granger 1963; 1980) and further developed by Geweke (Geweke, 1982) considers dependencies between L+1 successive values of X and Y, instead of single values. Let us assume that X_t, Y_t are independent of the past values of X and Y occurring before a time $t-L$, i.e., $X_{t-L-1}, X_{t-L-2}, \cdots$ and $Y_{t-L-1}, Y_{t-L-2}, \cdots$ This implies that one should only consider dependencies between X_t, Y_t and the L preceding values of the time series (Fig. 1a),

$$X_{t-1}^{(L)} \equiv X_{t-1}, X_{t-2}, ..., X_{t-L} \text{ and } Y_{t-1}^{(L)} \equiv Y_{t-1}, Y_{t-2}, ..., Y_{t-L} \quad (1)$$

The total information about X_t contained in Y is defined as the mutual information between the present of *X* and *Y* (present and past), $I(X_t : Y_t Y_{t-1}^{(L)})$ (Fig. 1b). By virtue of the identity $I(A : BC) = I(A : B) + I(A : C|B)$, the latter can be decomposed into an "instantaneous" and a "lagged" term:

$$I(X_t : Y_t Y_{t-1}^{(L)}) = I(X_t : Y_t | Y_{t-1}^{(L)}) + I(X_t : Y_{t-1}^{(L)}) \quad (2)$$

The conditioning on the instantaneous term implies that $I(X_t : Y_t | Y_{t-1}^{(L)})$ measures information about X_t contained exclusively in Y_t (and not already contained in $Y_{t-1}^{(L)}$). However, $I(X_t : Y_t Y_{t-1}^{(L)})$ possibly includes information that is already present in $X_{t-1}^{(L)}$. To obtain the "exclusive" information about X_t contained in Y we ought to condition over $X_{t-1}^{(L)}$ (Fig. 1c):

$$I(X_t : Y_t Y_{t-1}^{(L)} | X_{t-1}^{(L)}) \quad (3)$$

and again obtain an "instantaneous" and a "lagged" term:

$$I(X_t : Y_t Y_{t-1}^{(L)} | X_{t-1}^{(L)}) = I(X_t : Y_t | X_{t-1}^{(L)} Y_{t-1}^{(L)}) + I(X_t : Y_{t-1}^{(L)} | X_{t-1}^{(L)}) \quad (4)$$

The first term is called instantaneous causality (IC) and usually indicated by $F_{X\cdot Y}$ (Fig. 1d)

$$F_{X\cdot Y} \equiv I(X_t : Y_t | X_{t-1}^{(L)} Y_{t-1}^{(L)}) \quad (5)$$

The second term is called directed causality (DC) from Y to X and usually indicated by $F_{Y\to X}$ (Fig. 1e)

$$F_{Y\to X} \equiv I(X_t : Y_{t-1}^{(L)} | X_{t-1}^{(L)}) \quad (6)$$

Symmetrically, the exclusive information about Y_t contained in X is measured by

$$I(Y_t : X_t X_{t-1}^{(L)} | Y_{t-1}^{(L)}) = I(X_t : Y_t | X_{t-1}^{(L)} Y_{t-1}^{(L)}) + I(Y_t : X_{t-1}^{(L)} | Y_{t-1}^{(L)}) \quad (7)$$

The first term coincides with $F_{X\cdot Y}$ and the second one is the directed causality from X to Y (Fig. 1f),

$$F_{X\to Y} \equiv I(Y_t : X_{t-1}^{(L)} | Y_{t-1}^{(L)}) \quad (8)$$

The measures $F_{X\to Y}$, $F_{Y\to X}$ and $F_{X\cdot Y}$ were proposed by Geweke (Geweke, 1982), who also defined the total interdependence between X and Y as the sum of the three terms,

$$F_{X,Y} = F_{X\to Y} + F_{Y\to X} + F_{X\cdot Y} \quad (9)$$

This is the "new" correlation between X and Y created at time t, indeed

$$F_{X,Y} = I(X_t X_{t-1}^{(L)} : Y_t Y_{t-1}^{(L)}) - I(X_{t-1}^{(L)} : Y_{t-1}^{(L)}) \quad (10)$$

Granger causality measures can therefore be reformulated in completely information-theoretical terms (Barnett et al., 2009; Marko, 1973; Rissanen and Wax, 1987; Schreiber, 2000). Equivalent information-theoretic measures based on the Wiener-Granger principle, such as Transfer Entropy (Schreiber, 2000) and Directed Information (Massey, 1990), represent the most general measures of Wiener-Granger causality and capture any (linear and nonlinear) time-lagged conditional dependence between neural signals (Besserve et al., 2015; Vicente et al., 2011).

Covariance-based Granger Causality. The GC measures $F_{X\to Y}$, $F_{Y\to X}$ and $F_{X\cdot Y}$ capture statistical relations among the values of X, Y in a time window of length $L+1$ including the "present" values X_t, Y_t, and the "past" values $X_{t-1}^{(L)}, Y_{t-1}^{(L)}$. Together, $X_t, Y_t, X_{t-1}^{(L)}, Y_{t-1}^{(L)}$ define a vector of length $2L+2$ values. The GC measures can be

ultimately expressed in terms of Shannon entropies involving the ($2L+2$-variate) probability distribution $P(X_t, Y_t, X_{t-1}^{(L)}, Y_{t-1}^{(L)})$ and some of its marginals:

$$F_{X\to Y} = H(Y_t Y_{t-1}^{(L)}) - H(Y_{t-1}^{(L)}) - H(Y_t X_{t-1}^{(L)} Y_{t-1}^{(L)}) + H(X_{t-1}^{(L)} Y_{t-1}^{(L)}) \quad (11)$$

$$F_{X\cdot Y} = H(Y_t X_{t-1}^{(L)} Y_{t-1}^{(L)}) + H(X_t X_{t-1}^{(L)} Y_{t-1}^{(L)}) - H(X_{t-1}^{(L)} Y_{t-1}^{(L)}) - H(X_t Y_t X_{t-1}^{(L)} Y_{t-1}^{(L)})$$

Assuming the distribution $P(X_t, Y_t, X_{t-1}^{(L)}, Y_{t-1}^{(L)})$ to be stationary. The classical method to compute entropies is the "binning method". One considers T running windows of length $L+1$, and for each window extracts the vector $X_t, Y_t, X_{t-1}^{(L)}, Y_{t-1}^{(L)}$, thus obtaining T samples of $2L+2$. Binning each univariate variable and collecting the bin counts, the joint probability distribution $P(X_t, Y_t, X_{t-1}^{(L)}, Y_{t-1}^{(L)})$ is approximated by (multidimensional) histogram (Beirlant et al., 1997; Treves and Panzeri, 1995). If n bins are used for each univariate variable, the total number of multidimensional bins is $n^{2(L+1)}$. As a rule of thumb, to get at least a rough estimate of the bin counts one needs at least as many samples as bins, so $T \geq n^{2(L+1)}$ points. This requires a large sample $T \geq n^4$ for estimation. In order to make the estimation feasible on short time windows, a common solution is to approximate the distribution with the first term of the Gram-Charlier expansion, i.e., by a Gaussian distribution with the same second order moments (covariance matrix) as the given distribution. This approximation amounts to keeping only second order statistics, and neglecting higher-order terms, and is rather accurate for fMRI data (Hlinka et al., 2011). In this approximation, the distribution $P(X_t, Y_t, X_{t-1}^{(L)}, Y_{t-1}^{(L)})$ and its marginals are effectively replaced by the covariance matrix $\Sigma(X_t, Y_t, X_{t-1}^{(L)}, Y_{t-1}^{(L)})$ and its submatrices. Estimating Σ requires only to estimate $(2L+2)^2$ parameters corresponding to the second moments of the distribution. Furthemore, entropies can be simply computed with the formula

$$H(A) = \frac{n_A}{2} log\ 2\pi e + \frac{1}{2} log|\Sigma(A)| \quad (12)$$

where $\Sigma(A)$ is the covariance matrix of A, n_A the dimension of A, and $|\cdot|$ is the determinant. Thus, in this *covariance-based* approximation, GC measures are expressed in terms of determinants of submatrices of the covariance matrix of the data (Brovelli et al., 2015). For instance,

$$F_{X\to Y} = \frac{1}{2}log|\Sigma(Y_t Y_{t-1}^{(L)})| - \frac{1}{2}log|\Sigma(Y_t)| + \\ - \frac{1}{2}log|\Sigma(Y_t X_{t-1}^{(L)} Y_{t-1}^{(L)})| + \frac{1}{2}log|\Sigma(X_{t-1}^{(L)} Y_{t-1}^{(L)}))| \quad (13)$$

The covariance-based GC estimation is equivalent to the parametric estimation of GC from an autoregressive model with Gaussian innovations, i.e., the traditional way to estimate Granger causality.

Gaussian-copula-based estimation of GC. The assumption of Gaussianity can be relaxed as follows. If two variables X, Y are not Gaussian, one may nevertheless be able to find two new variables $\tilde{X}, \tilde{Y}$ that are Gaussian and have the same MI as X, Y. One can then apply the covariance-based estimation to $\tilde{X}, \tilde{Y}$. The GC measures $F_{X\to Y}$, $F_{Y\to X}$ and $F_{X\cdot Y}$ can be written as appropriate sums of mutual information (MI) terms. For instance,

$$F_{X\to Y} = I(Y_t : X_{t-1}^{(L)} | Y_{t-1}^{(L)}) = I(Y_t : X_{t-1}^{(L)} Y_{t-1}^{(L)}) - I(Y_t : Y_{t-1}^{(L)}) \quad (14)$$

The MI is invariant under monotonic transformations of the marginals. Formally, consider the transformations

$$\tilde{X} = t(X), \ \tilde{Y} = u(Y) \quad (15)$$

where t, u are monotonic functions: it holds that $I(X : Y) = I(t(X) : u(Y))$. The invariance is exploited in the Gaussian copula estimation of mutual information (Ince et al., 2017). In short, one first transforms the marginals such that they are Gaussian, and then applies a covariance-based MI estimation to the transformed variables. In detail, consider two random variables X, Y with joint cumulative distribution function (CDF) $H(X, Y)$ and marginal CDFs $F(X)$, $G(X)$. Consider

$$t(X) = \Phi^{-1}(F(X)), \ u(Y) = \Phi^{-1}(G(Y)) \quad (16)$$

where Φ is the CDF of a standard normal variable. One can immediately show that $\tilde{X} = t(X)$, $\tilde{Y} = u(Y)$ are standard normal variables, i.e., $\tilde{F}(\tilde{X}) = \Phi(\tilde{X})$, $\tilde{G}(\tilde{Y}) = \Phi(\tilde{Y})$. Applying the covariance-based approach to the transformed variables, one has $I(\tilde{X}, \tilde{Y}) = \frac{1}{2}log\frac{|\Sigma_{\tilde{X}}||\Sigma_{\tilde{Y}}|}{|\Sigma_{\tilde{X}\tilde{Y}}|}$, and by virtue of the invariance $I(X, Y) = I(\tilde{X}, \tilde{Y})$. The Gaussian evaluation of the MI between $\tilde{X}, \tilde{Y}$ is not exact. In general, even though the marginal distribution of $\tilde{X}, \tilde{Y}$ are Gaussian, the joint distribution is not a bivariate Gaussian. This

is true only if the *copula*, i.e., the part of the distribution specifying the dependence between the two variables, is Gaussian (see Ince et al. 2017 for a definition of copula and discussion of this point). However, for many distributions the Gaussian copula assumption is approximately met. In summary, one obtains the following algorithm to compute the MI: i) given samples $\{X_i, Y_i\}$, approximate $F(X)$, $G(Y)$ with the empirical CDFs $F(X_i) = rank(X_i)/N$, $G(Y_i) = rank(Y_i)/N$ and compute $t(X_i) = \Phi^{-1}(rank(X_i)/N)$, $u(Y_i) = \Phi^{-1}(rank(Y_i)/N)$. $t(X_i)$ and $u(Y_i)$ are normally distributed and have the same MI as X_i, Y_i ii) compute the MI from the samples $\{t(X_i), u(Y_i)\}$ with the covariance-based method. In our work, we have computed all GC measures by expressing them in terms of sums of MIs and then applying the Gaussian-copula-based estimation to each term in the sum.

Overall, the first advantage of bivariate gaussian-copula and covariance-based GC is its applicability to large networks of nodes, such as the 343 nodes used in this study. Most other methods to infer directed GC (such as multivariate Granger causality) are more accurate in inferring *direct* (i.e., non-mediated) influences, but usually applicable to only smaller networks (of the order of 100 nodes) (Tang et al., 2012; Stramaglia et al., 2016). The use of covariance-based GC does not require to select a specific sub-network of nodes, or to average BOLD signals over large regions (which would imply a considerable signal loss, due to potential inhomogeneities). A second advantage is its estimability from short signals. This property allows us to estimate GC from BOLD time series of 400-800 time points, i.e., the time series of single subjects. Thus, we do not need to concatenate several subjects to perform the estimation, and we can obtain individual estimates. These two key properties enable a direct comparison of Granger causality results with previous FC studies.

Choice of the appropriate lag (L). GC measures $F_{X\to Y}$, $F_{Y\to X}$ and $F_{X\cdot Y}$ depend on the time window length L used to define the past of each time series. Intuitively, L should include all points in the past that have correlations with X_t, Y_t. This would roughly correspond to the autocorrelation decay time of the time series. For rs-fMRI, this is of the order of 10s (5 TR). More rigorously, we tested how many points in the past significantly contribute to predicting the present values of the time series by assuming a

specific form for the process generating the data. If we assume that the data are generated by a Gaussian vector autoregressive (VAR) process of length L

$$X_t = \sum_{s=1}^{L} a_{xx,s} X_{t-s} + a_{xy,s} Y_{t-s} + \varepsilon_x \,, \quad Y_t = \sum_{s=1}^{L} a_{yx,s} X_{t-s} + a_{yy,s} Y_{t-s} + \varepsilon_y \tag{17}$$

where ε_x, ε_y are (possibly correlated) Gaussian innovations. This can be rewritten as

$$X_t = A_{xx} \cdot X_{t-1}^{(L)} + A_{xy} \cdot Y_{t-1}^{(L)} + \varepsilon_x \,, \quad Y_t = A_{yx} \cdot X_{t-1}^{(L)} + A_{yy} \cdot Y_{t-1}^{(L)} + \varepsilon_y \tag{18}$$

with $L \times 1$ vectors $A_{xx}, A_{xy}, A_{yx}, A_{yy}$. In this setting X_t, Y_t are Gaussian with means $\mu_x = A_{xx} X_{t-1}^{(L)} + A_{xy} Y_{t-1}^{(L)}$, $\mu_y = A_{yx} X_{t-1}^{(L)} + A_{yy} Y_{t-1}^{(L)}$ and covariance σ given by the 2×2 covariance matrix of $\varepsilon_x, \varepsilon_y$. Using least squares estimation, one obtains the best fit for the parameters

$$A_{xx,s} = \frac{cov(X_t, X_{t-s})}{var(X_{t-s})} \,, A_{xy,s} = \frac{cov(X_t, Y_{t-s})}{var(Y_{t-s})} \,, A_{yx,s} = \frac{cov(Y_t, X_{t-s})}{var(X_{t-s})} \,,$$
$$A_{yy,s} = \frac{cov(Y_t, Y_{t-s})}{var(Y_{t-s})} \,, \sigma = \Sigma(X_t Y_t | X_{t-1}^{(L)} Y_{t-1}^{(L)}) \tag{19}$$

where $\Sigma(A|B) = \Sigma(A) - \Sigma(X,Y)\Sigma^{-1}(B)\Sigma(A,B)^T$ is the partial covariance matrix of A given B, with $det\,\sigma = |\Sigma(X_t Y_t, X_{t-1}^{(L)} Y_{t-1}^{(L)})| - |\Sigma(X_{t-1}^{(L)} Y_{t-1}^{(L)})|$.

An appropriate choice of L is given by model comparison, i.e., by fitting models with different L to the data and selecting the model yielding the "best fit". Since the models for increasing L are nested (models with higher L include models with lower L as a special case), the likelihood of the models increases monotonically as a function of L. To avoid overfitting, the customary procedure with nested models is to select the proper L by a model-comparison criterion penalizing models with a larger number of parameters. Here, we used the common BIC criterion (McQuarrie and Tsai, 1998) that assesses the fitness of each model as $B = 2log\Lambda - d\,log(n)$ where Λ is the log-likelihood, and $d\,log(n)$ is a term penalizing models with a large number of parameters d. The log-likelihood of the model (17) is $log\Lambda = -\frac{N}{2} log 2\pi e\, det\,\sigma$ which gives the BIC value

$$BIC = d\,log(n) - 2log\Lambda = 4(L+1)\,log(n) - \frac{N}{2} log 2\pi e\, det\Sigma(X_t Y_t | X_{t-1}^{(L)} Y_{t-1}^{(L)}) \tag{20}$$

The best-fitting model is the one maximising BIC. We computed the value of BIC for all pairs of regions-of-interest (ROIs) and all subjects (patients and controls) as a function of L. We found that on average BIC increases up to $L \approx 5$, and then remains

relatively stable. Note that since TR= 2s, $L = 5$ corresponds to the expected autocorrelation length of the signal. On the basis of these results, we chose to fix $L = 5$ in our analyses.

Relation between linear correlation and covariance-based Granger causality measures. Standard undirected functional connectivity (UFC) is classically computed as the Pearson's correlation, defined as $R = \frac{\sigma(X,Y)}{\sigma(X)\sigma(Y)}$ where $\sigma(X)$, $\sigma(Y)$ are the standard deviations of X_t and Y_t and $\sigma^2(X,Y)$ is their covariance within the selected time window. The UFC only considers dependencies between X_t and Y_t for the same *t.* UFC and covariance-based Granger causality measures share common properties. Linear correlation and total interdependence are undirected measures quantifying static and dynamic dependencies, respectively. Although these measures are not related by a mathematical decomposition, there is a strong relationship between the existence of both types of dependencies. A lack of total interdependence implies a lack of linear correlation; and, if we assume that the future of X and Y causally depends on their own past, respectively, the opposite relation is also true. This occurs because linear correlation is related to the covariance-based approximation of the mutual information, $I(X_t : Y_t) = -1/2 log(1 - R^2)$, and because conditioning on the past cannot create new dependencies (Chicharro and Panzeri, 2014). It is also clear the directed and instantaneous Granger measures are smaller than the total interdependence. Thus, null total interdependence implies the absence of Granger causality measures because they constitute non-negative contributions to the total interdependence. In other words, Granger causality is present if, and only if, both linear correlation and total Granger interdependencies are not zero.

The FC and GC quality-based exclusion criteria. In order to ensure good-quality FC and GC estimates, we excluded from analysis all subjects with less than 400 usable frames after motion scrubbing. Furthermore, for each subject, we computed a lag between homologous ROIs as in (Siegel et al., 2016B). In brief, for any integer lag $l = -4, -3, ..., 3, 4$ we computed the lagged cross-correlation $C_l = < X_t Y_{t+l} >$ between

the BOLD signals X, Y of the homologous ROIs; the homotopic lag between the ROIs was identified by finding $l_0 = argmin(C_l)$, performing a parabolic interpolation on C_{l_0-1}, C_{l_0}, C_{l_0+1}, and computing the minimum of the parabola. An average homotopic lag between the left and right hemisphere was computed by averaging over all homptipic lags between left ROIs and the homologous right ROIs. Anomalously large homotopic lags are a likely indication of the presence of lags of hemodynamic origin, due to disruption of the standard hemodynamic response in the vicinity of the lesion. Therefore, we excluded from analysis all subjects with severe homotopic lags (greater than 1s inter-hemispheric difference). After motion and lag exclusion, 113 patients were included at two weeks, 27 controls at time point one, and 25 at time point two.

RESULTS

We analyzed resting-state fMRI data of acute stroke patients (n=113) and healthy control subjects (n=26). Our analysis tested the hypothesis that post-stroke FC alterations are tightly intertwined with information flow deficits occurring both inter-hemispherically and intra-hemispherically. To address this issue, we performed covariance-based Granger causality analyses (Brovelli et al., 2015) of resting-state fMRI data and compared inter-areal information flow analyses with standard FC approaches. The comparison was performed by means of the notion of total interdependence between signals (Geweke et al., 1982). In the GC framework, the total interdependence between two signals can be split into three terms: two directed Granger causality (DC) terms and an instantaneous Granger causality (IC) term. The DC terms ($F_{X\to Y}$, $F_{Y\to X}$) represent a directed flow of information from X to Y or vice versa. The IC term ($F_{X\cdot Y}$) represents information shared between X and Y "instantaneously", i.e., in less than one TR, and it accounts for unconsidered influences that may originate from common (e.g., subcortical) sources. Functional MRI data were computed for 324 parcels of the Gordon-Laumann cortical parcellation (Gordon et al., 2016) and 19 sub-cortical and cerebellar parcels from the FreeSurfer atlas (Fischl et al., 2002). For each subject and for each pair of regions-of-interest (ROIs), we evaluated the undirected functional connectivity (UFC, z-transformed Pearson correlation), the instantaneous Granger causality (IC) and the directed Granger causality in both directions (DC). For control subjects, the DC, IC and UFC matrices obtained in two independent sessions were averaged. We then investigated differences in DC and IC (i) between the two hemispheres and (ii) within the lesioned and intact hemisphere, and compared the results with shifts in UFC.

Consistency of UFC and GC measures across fMRI sessions

We first tested the reliability of our results by verifying the consistency of the UFC and GC measures obtained for control subjects in two separate sessions (Fig. 2a). Consistency was defined as the Pearson correlation between the (upper-triangular parts

of the) corresponding matrices in the two sessions. The UFC matrices were highly consistent (r=0.65±0.03, average and standard error over subjects). The same result was obtained for IC matrices (r=0.73±0.02). The DC matrices, instead, were much less consistent (r=0.22±0.02). We obtained reduced network-wise (28×28) FC matrices by averaging over ROIs in the same network and hemisphere. We considered thirteen cortical resting-state networks as in (Gordon et al., 2016), plus subcortical ROIs. Consistency improved for UFC (r= 0.80±0.03), IC (r=0.87±0.03), and DC (r=0.41±0.03). The UFC and DC results are thus reliable at the single-subject level, especially if network-averaged results are considered. As for the DC, due to the poor level of consistency obtained in the full (343×343) DC matrix, we cannot expect reliable results at the level of single subject, single ROI. Also at the network level individual results are not completely reliable. To assess the reliability of group results, we computed the consistency of group-averaged FC matrices for random groups of n subjects (Fig. 2b). The group consistency is significantly stronger than the individual consistency. When considering groups of 5 subjects, the DC consistency rises to 0.4 (0.7 for network-wise matrices), and for 10 subjects it rises to 0.5 (0.8 for network-wise matrices). This result implies that while individual DC results are affected by a very large noise, DC results at the group-level are reliable. In summary, UFC and IC matrices were highly consistent both at the individual and group level, while DC matrices were consistent only at the group level.

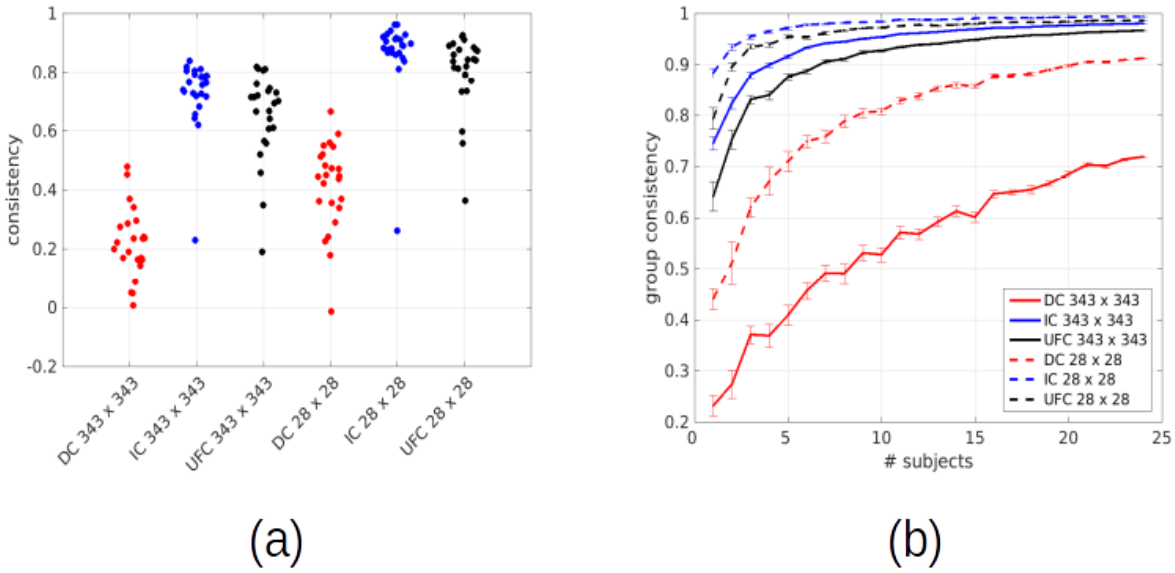

Figure 2: Consistency of FC measures in two separate sessions. We computed 343×343 DC, IC and UFC matrices for the two separate sessions of control subjects. We assessed consistency between the FC results in the two sessions as the Pearson correlation between the (upper-triangular part of the) corresponding matrices in the two sessions. We also evaluated consistency between the 28×28 DC, IC and UFC matrices obtained by averaging over all pairs of ROIs belonging to the same RSN (13 cortical resting state systems + subcortical ROIs). In panel (a) we show the distribution of consistency for the individual results of each subject. In panel (b), we assess consistency of group averages. For each *n*, we randomly select *n* subjects and average the FC matrices over subjects. We then show the average (over random choices of n subjects) consistency of the group-averaged matrices as a function of *n*

Interhemispheric homotopic undirected functional connectivity and Granger causality analyses

Previous studies have shown that stroke patients present a reduced interhemispheric UFC with respect to healthy controls (Carter et al., 2010; Golestani et al., 2013; He et al., 2007; New et al., 2015; Park et al., 2011; Ramsey et al., 2016; Siegel et al., 2016; Tang et al., 2016). Such effect is strongest for interhemispheric homotopic connections, which link homologous ROIs located symmetrically in opposite hemispheres. We computed UFC, IC, and DC between pairs of homologous ROIs and compared healthy controls with stroke patients. Furthermore, we subdivided the latter group into patients with lesions in the left hemisphere (LH patients) and patients with lesions in the right

hemisphere (RH patients). LH and RH patients were kept separate as they were clinically different and presented dissimilarities in FC.

Global measures of homotopic connectivity were obtained by averaging the UFC, IC and DC over all pairs of homotopic links. Network-wise measures were obtained by averaging over pairs of homotopic ROIs belonging to the same resting state network (RSNs). We considered twelve RSNs as in (Gordon et al., 2016), in addition to subcortical regions, and left out networks with less than 5 nodes. We considered the following RSNs: the visual network (VIS), sensorimotor dorsal network (SMD), sensorimotor ventral network (SMV), auditory network (AUD), cingulo-opercular network (CON), ventral attention network (VAN), dorsal attention network (DAN), default mode network (DMN), fronto-parietal network (FPN), subcortical regions (SUB).

Figure 3a shows the distribution of the homotopic UFC, averaged over all homotopic pairs for healthy controls (n=26), LH patients (n=60) and RH patients (n=53) in the sub-acute phase. We observed a significant difference in the UFC distribution between the three groups (one-way ANOVA, $F(2,136)=6.6$, $p=0.002$). Post-hoc T-tests show that the UFC was significantly higher in controls as compared to LH patients ($T(84)=4.1$, $p=0.0001$) and RH patients ($T(77)=3.2$, $p=0.0001$), which in turn were not different (LH vs. RH patients $T(111)=-0.9$, $p=0.37$). Figure 4d shows UFC distributions for each RSN. We found a significant effect of group and network, as well as a significant group x network interaction (two-way ANOVA; group: $F(2,1224) = 6.4$, $p=0.002$; network: $F(9,1224) = 126.7$, $p < 10^{-10}$; interaction: $F(18,1224) = 2.1$, $p= 0.005$). Post-hoc T-tests showed that controls had significantly higher UFC than LH patients ($p<0.05$ FDR corrected for 10 comparisons) in all networks except for the VAN, and significantly higher UFC than RH patients in all networks except for the VAN, DMN, FPN and SMV ($p<0.05$ FDR corrected for 10 comparisons). The UFC appeared to be slightly higher for RH than LH patients; however, the difference between LH and RH patients disappeared (one-way ANOVA: $F(1,1110) = 1.5$, $p= 0.2$) if controlled for lesion volume by linearly regressing the logarithm of volume lesion from the UFC. In summary, stroke patients presented an overall decrease of homotopic UFC with respect to healthy subjects, with a stronger effect for patients with larger lesion volume. The effect was strongest for homotopic connections in VIS, SMD, AUD, CON, DAN networks, and for subcortical

regions. Analogous results were already obtained in previous analyses (Joshua Sarfaty Siegel et al., 2016).

The analysis of homotopic UFC in patients showed that the activity of homologous regions is less correlated than in healthy controls, suggesting a reduced interaction between the hemispheres. Granger causality (GC) analyses were performed to characterize instantaneous (IC) and directional (DC) interactions between homologous regions. Figure 3b depicts the distribution of instantaneous causality (IC), averaged over all homotopic pairs of ROIs. We observed a significant difference in IC between the three groups of subjects (one-way ANOVA, $F(2,136) = 14.0$, $p = 3 \cdot 10^{-6}$). Post-hoc t-tests showed that the IC was significantly higher in controls with respect to LH patients ($T(84) = 5.5$, $p = 4 \cdot 10^{-6}$) and RH patients ($T(77) = 4.2$, $p = 0.0001$), but did not differ between LH and RH patients ($T(111) = -1.1$, $p = 0.27$). Figure 3e shows results separately for each network. We found significant effects both for group type and networks, as well as a group x network interaction (two-way ANOVA; group: $F(2,1224) = 13.5$, $p = 4 \cdot 10^{-6}$; network: $F(2,1224) = 180.3$, $p < 10^{-10}$; interaction: $F(18,1360) = 4.2$, $p = 1.0 \cdot 10^{-10}$). While controls had significantly higher IC than both LH and RH patients in all networks (t-test, $p < 0.05$ FDR corrected for 10 comparisons), the strongest differences between patients and controls was observed in the VIS, SMD, CON, DAN and subcortical regions. Similarly to UFC, the IC was slightly higher for RH than LH patients, but controlling for lesion volume removed the effect (one-way ANOVA: $F(1,1110) = 3.4$, $p = 0.06$). In summary, the IC results are in qualitative agreement with those of UFC, but the discrepancy between patients and control subjects is more pronounced (as mirrored in a larger group effect).

We then analyzed directional Granger causality measures between homologous regions. We first investigated whether the bidirectional information flow across hemispheres was different between patients and controls. To this aim, we computed total directed interdependence between brain regions, defined as the sum of DC estimates, $S_{X \leftrightarrow Y} = F_{X \to Y} + F_{Y \to X}$ where X is a ROI in the left hemisphere and Y the homologous ROI in the right hemisphere. Figure 3c shows the distribution of the homotopic bidirectional DC, averaged over homotopic pairs of regions. We observed a significant difference between the three groups (one way Anova, $F(2,136) = 3.6$, $p = 0.03$);

post-hoc t-tests show that the homotopic DC was significantly higher in controls than LH patients (T(84)=2.9, p=0.006), but not RH patients (T(77)=1.2, p=0.22). Considering different networks separately (Fig. 3f), we found a significant effect of group and network separately (group: F(2,1224)=3.7, p=0.03; network: F(9,1224)=75.8, $p<10^{-10}$; interaction: F(18,1224)=1.3, p=0.14). For all networks, the bidirectional information flow was higher in healthy controls than LH patients.

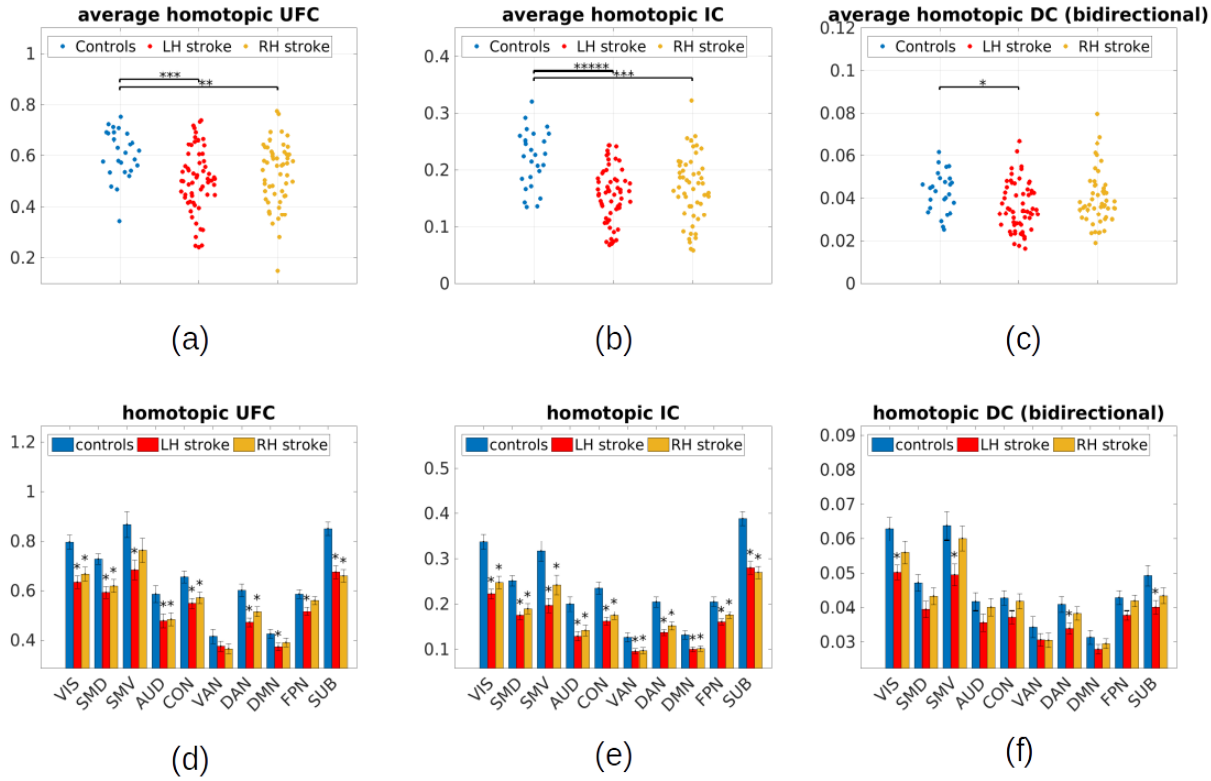

Figure 3: Average homotopic UFC, IC and DC in acute phase. For each subject, we averaged the UFC, the IC, and the bidirectional DC for homotopic pairs of ROIs. (a-c) show individual averages of homotopic UFC, IC, bidirectional DC (each dot represents one subject). At a group level, the average homotopic UFC and IC are higher for controls than both LH and RH patients. The bidirectional DC is higher for controls than LH patients. (d-f) show homotopic UFC, IC and bidirectional DC by resting-state network. Column heights are averages over subjects, error bars standard errors over subjects. At the group level, the UFC and IC for each network is higher in controls compared to patients. Control/patient differences are stronger for IC than UFC. The average bidirectional DC for each network is higher in controls compared to LH patients. Stars indicate networks for which comparison with controls (two-sample T-test, p<0.05 FDR corrected for 10 comparisons) is significant. VIS=visual, SMD=sensorimotor dorsal,

SMV=sensorimotor ventral, AUD=auditory network, CON=cingulo-opercular network, VAN=ventral attention network, DAN=dorsal attention network, DMN=default mode network, FPN=fronto-parietal network SUB=subcortical nodes.

We then studied whether stroke induces an asymmetry in information flow between the hemispheres by quantifying the asymmetry in information flow between brain regions, defined as the difference in DC, $G_{X\to Y} = F_{X\to Y} - F_{Y\to X}$. We computed the net homotopic DC asymmetry $G_{X\to Y}$ where X is a ROI in the right hemisphere and Y the homologous ROI in the left hemisphere. $G_{X\to Y}$ larger than zero implies a net information flow from the right to the left hemisphere, and vice versa for $G_{X\to Y}$ smaller than zero. Figure 4a shows the distribution of the homotopic DC asymmetry, averaged over homotopic pairs of ROIs. We observed a significant difference between the three groups (one-way ANOVA, $F(2,136)=13.5$, $p=4\cdot10^{-6}$). Post-hoc t-tests showed that the net homotopic information flow is shifted towards the left hemisphere in LH patients compared to control subjects ($T(84)=3.1$, $p=0.002$), and significantly shifted towards the right hemisphere in RH patients compared to controls ($T(77)=2.5$, $p=0.02$). In other words, the DC from the intact to the lesioned hemisphere tended to be higher than in the opposite direction, implying a net information flow from the intact to the lesioned hemisphere. Considering individual RNSs (Fig. 4d), we found significant effects at the group and network level (group: $F(2,1224)=11.1$, $p=4\cdot10^{-5}$; network: $F(9,1224)=2.3$, $p=0.02$; interaction: $F(18,1224)=1.2$, $p=0.2$). For all networks, the information flow captured by the DC asymmetry was higher from the healthy to the lesioned hemisphere in patients. Figure 4d additionally shows that the net information flow in healthy participants was preferentially from the left (dominant) towards the right (non-dominant) hemisphere, but the net asymmetry was much weaker than that observed in patients.

We then investigated whether the asymmetry effect could be attributed to a reduction of DC from the lesioned to the intact hemisphere, or rather to an enhancement of DC from the intact to the lesioned hemisphere. We analysed separately homotopic DC terms $F_{X\to Y}$, $F_{Y\to X}$ where X is a ROI in the left hemisphere and Y the homologous ROI in the right hemisphere. The results revealed that the asymmetry is due to a reduction of DC from the lesioned to the healthy hemisphere. Indeed, we found that the homotopic

DC from the lesioned to the healthy hemisphere (left to right) in LH patients was significantly lower than in healthy controls ($T(84)=3.9$, $p= 3\cdot10^{-4}$), while the DC from the healthy to the lesioned hemisphere (right to left) was only slightly, but not significantly reduced ($T(84)=1.6$, $p=0.1$) (see Fig. 4b-4c). For RH patients, the DC from the lesioned to the healthy hemisphere (right to left) was significantly lower in comparison with healthy controls ($T(77)=2.2$, $p=0.03$), while the DC from the healthy to the lesioned was comparable ($T(77)=-0.05$, $p=0.95$). In Fig. 4e and 4f, we show the DC from left to right and from right to left for different networks, respectively. We performed a three-way ANOVA to test for the effects of group, network and directionality (left to right vs right to left) on homotopic DC. We found a significant effect of group ($F(2,136)=3.7$, $p=0.03$), network ($F(9,2584)=74.9$, $p<10^{-10}$) and directionality ($F(1,2584)=5.7$, $p=0.02$), as well as significant group x directionality ($F(2,2584)=37.8$, $p<10^{-10}$) and network x directionality ($F(9,2584)=2.5$, p-0.01) effects. In summary, the homotopic directed connectivity from the lesioned to the intact hemisphere was reduced with respect to healthy controls. Directed connectivity from the intact to the lesioned was slightly reduced (for LH patients) or comparable with that of healthy controls. Consequently, stroke patients present an asymmetric interhemispheric information flow, going from the healthy to the lesioned hemisphere.

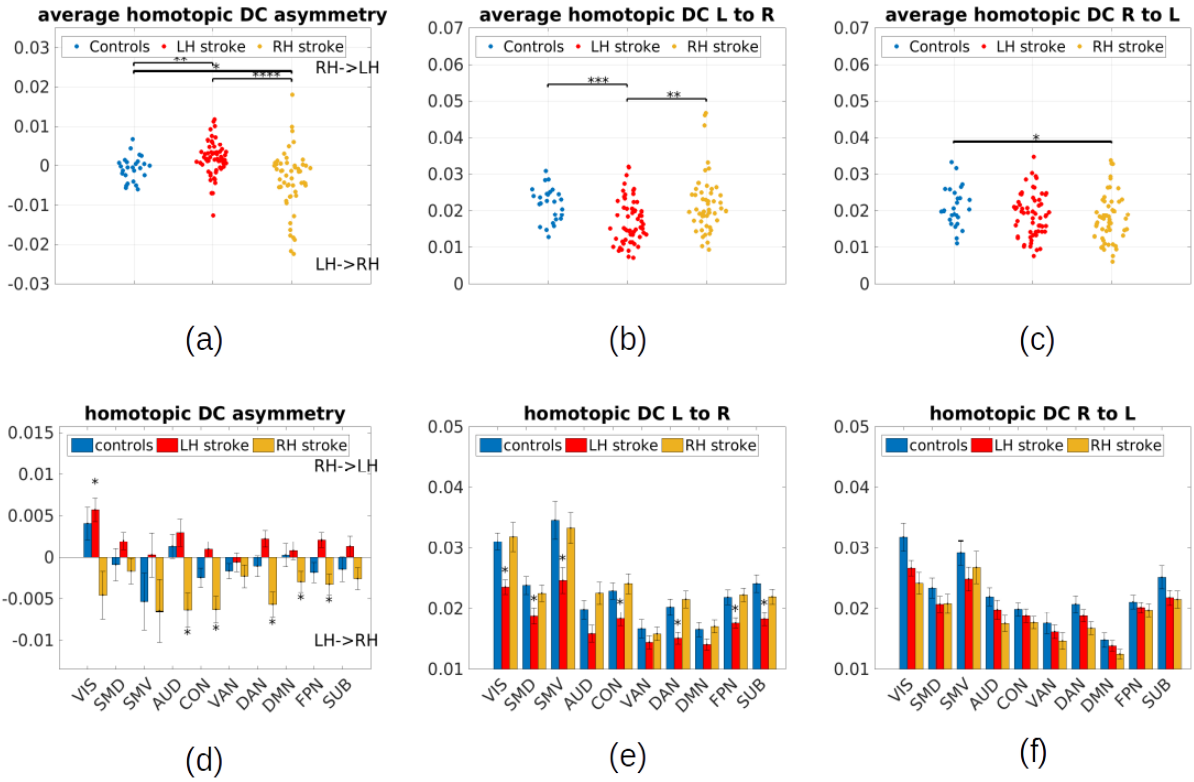

Figure 4: Direction of the average homotopic DC in acute phase. For each subject, we averaged the DC over homotopic pairs of ROIs, considering separately the DC from left regions to right regions, from right regions to left regions, and the difference, called homotopic DC asymmetry asymmetry. (a-c) we show individual averages of homotopic DC from left to right, right to left, and asymmetry (left to right - right to left). Each dot represents a subject. At a group level, for both LH and RH patients, the information flow (DC asymmetry) is in the direction of the lesioned hemisphere, i.e., the homotopic DC from the intact to the lesioned hemisphere is higher than vice versa. DC from left to right is reduced for all patients compared to controls, but much more strongly for LH patients. DC from right to left is reduced for RH patients compared to controls. Overall, DC from the lesioned to the intact hemisphere tends to be reduced in patients. (d) We show homotopic DC asymmetry (right to left - left to right) by resting-state network. Column heights are averages over subjects, error bars standard errors over subjects. For all networks, the information flow (DC asymmetry) is from right to left LH patients, and from left to right in RH patients. Stars represent networks for which comparison with 0 (one-sample T-test, $p<0.05$ FDR corrected for 10 comparisons) is significant. (e-f) We show homotopic DC from left to right and right to left. Column heights are averages over subjects, error bars standard errors over subjects. DC from left to right is significantly reduced in several networks for LH patients. Stars represent networks for which comparison with controls (two-sample T-test, $p<0.05$ FDR corrected for 10 comparisons) is significant. VIS=visual, SMD=sensorimotor dorsal, SMV=sensorimotor ventral, AUD=auditory network, CON=cing VIS=visual, SMD=sensorimotor dorsal, SMV=sensorimotor ventral, AUD=auditory network,

CON=cingulo-opercular network, VAN=ventral attention network, DAN=dorsal attention network, DMN=default mode network, FPN=fronto-parietal network SUB=subcortical nodes.

Intra-hemispheric undirected functional connectivity and Granger causality analyses

We then investigated intra-hemispheric UFC, IC, and DC. Previous studies have shown that brain damage leads to a bilateral increase of intra-hemispheric functional connections (Baldassarre et al., 2014; Eldaief et al., 2017; Ramsey et al., 2016; Siegel et al., 2016). Our analysis, however, showed that the increase of intra-hemispheric UFC is, on average, subtle. Figure 5a shows the total (left and right) intra-hemispheric UFC for healthy controls and stroke patients. The group effect was not significant (one-way ANOVA, $F(2,136) = 2.2$, $p= 0.12$), and post-hoc T-tests revealed only a marginally significant increase for both LH patients ($T(84)=2.08$, $p=0.04$) and RH patients ($T(77)=2.24$, $p=0.03$) in comparison to controls. When considering different resting-state networks separately (for each network, we considered the sum of its connections with all networks), we obtained consistent results (Figure 5d). We found a significant effect of network only, not group (two-way ANOVA; group: $F(2,1224)=1.5$, $p=0.2$; network: $F(9,1224)=259.3$, $p<10^{-10}$; interaction: $F(18,1224)=0.8$, $p=0.7$).

We then investigated whether stroke impacts the balance in intra-hemispheric functional connectivity between the lesioned and intact hemisphere. We computed a measure of intra-hemispheric imbalance defined as the difference between the mean UFC averaged over all pairs of regions within the same hemisphere. The intra-hemispheric UFC did not show a significant imbalance between lesioned and healthy hemisphere (Fig. 5g). The three groups did not show a significant difference in imbalance (one-way ANOVA, $F(2,136)=0.97$, $p=0.38$). Post-hoc T-tests did not show differences in UFC imbalance between any pair of groups (controls compared to LH patients ($T(84)=0.27$, $p=0.78$), controls compared to RH patients ($T(77)=1.425$, $p=0.15$), and LH compared to RH patients ($T(111)=1.1$, $p=0.27$).

Contrary to UFC, the mean intra-hemispheric IC was clearly reduced in patients as compared to controls. Compared to healthy controls, LH patients presented instead a reduced intra-hemispheric IC in both hemispheres (Fig 5h and 5i), with a more pronounced reduction in the lesioned one (left: $T=-3.0$, $p=0.004$; right: $T=-2.17$,

p=0.03). In RH patients, the IC was reduced only in the lesioned hemisphere (left: T=−0.7, p=0.48; right: T=−2.31, p=0.02; Fig. 5h and 5i). To conclude, the IC presented an imbalance between the two hemispheres in stroke patients. Figure 5b shows the distribution of the intra-hemispheric IC imbalance (difference between the average intra-hemispheric IC in right and left hemisphere) for LH/RH patients and controls. The three groups are significantly inhomogeneous (one-way ANOVA, F(2,136)=19.6, $p=3\cdot10^{-8}$), with significant differences pairwise in controls compared to LH patients (T(84)=−2.5, p=0.01), controls compared to RH patients (T(77)=3.7, p=0.0004), and LH compared to RH patients(T(111)=5.7, $p=1\cdot10^{-7}$). Figure 5e shows the intra-hemispheric IC imbalance for different resting state networks. For each network, we considered the sum of its connections with all networks. We found a significant effect of group and network, as well as a significant interaction (group: F(2,1224)=19.7, $p<3\cdot10^{-8}$; network: F(9,1224)=5.4, $p=2\cdot10^{-7}$; interaction: F(18,1224)=4.1, $p=2\cdot10^{-8}$). We observed a significant (T-test, p<0.05 FDR corrected) imbalance for both LH and RH patients in the AUD, CON and DAN networks. For RH patients, we found an imbalance also in VIS, SMD, SMV, DMN and FPN. The stronger effects observed in RH patients could be explained by lesion volume, as LH patients have wider lesions than RH patients. Healthy subjects presented a significant imbalance in the VAN and FPN (i.e., the IC was higher in the left hemisphere). In summary, stroke patients showed lower intra-hemispheric IC in the lesioned hemisphere than the intact one. Compared to healthy subjects, the intra-hemispheric IC was found to be lower in both hemispheres (more severely in the lesioned one) for LH patients and in the lesioned hemisphere for RH patients.

Finally, we analyzed DC within each hemisphere and computed a bidirectional DC strength, defined as $S_{X\leftrightarrow Y} = F_{X\rightarrow Y} + F_{Y\rightarrow X}$. This metric was computed over all pairs of ROIs within each hemisphere. Compared to healthy controls, LH patients presented a slight, but non-significant (left: T=−1.6, p=0.10), reduction in intra-hemispheric DC in the left hemisphere, but not in the right hemisphere (right: T=−0.84, p= 0.40). RH patients presented no significant difference either (left: T=−0.28, p= 0.77; right: T=−0.59, p= 0.55). All groups presented an imbalance in intra-hemispheric DC (Figure 5c). For LH patients, the intra-hemispheric DC was higher in the right (healthy) hemisphere. For RH

patients and controls the intra-hemispheric DC was higher in the left hemisphere, which is the dominant hemisphere for healthy subjects and the healthy hemisphere for RH patients. The three groups were significantly inhomogeneous (one-way ANOVA, $F(2,136)=8.12$, $p=5\cdot10^{-4}$), with significant differences pairwise in controls compared to LH patients ($T(84)=-3.3$, $p= 0.0016$), and LH compared to RH patients ($T(111)=3.6$, $p=0.0005$). We did not observe a significant difference in controls compared to RH patients ($T(77)=1.0$, $p=0.34$). The left-ward imbalance effect appeared only slightly strengthened in RH patients compared to control subjects. In Figure 5f, we show the imbalance in intra-hemispheric DC for different resting state networks. For each network, we considered the sum of its incoming and outgoing connections with all other networks. We found a significant effect of group and network, as well as a significant group x network interaction (two-way ANOVA; group: $F(2,1224)=8.9$, $p=0.0002$; network: $F(9,1360)=3.7$, $p=0.0001$; interaction: $F(18,1224)=2.6$, $p=0.0002$). We observed a significant (T-test, $p<0.05$ FDR corrected) imbalance in CON, AUD and DMN and subcortical regions for both LH and RH patients. Additionally, RH patients had a significant imbalance in VIS, VAN and FPN networks. We observed an imbalance in VIS, VAN, FPN and the CON networks also for healthy controls, so the RH patients' effect may not be an anomaly related to stroke.

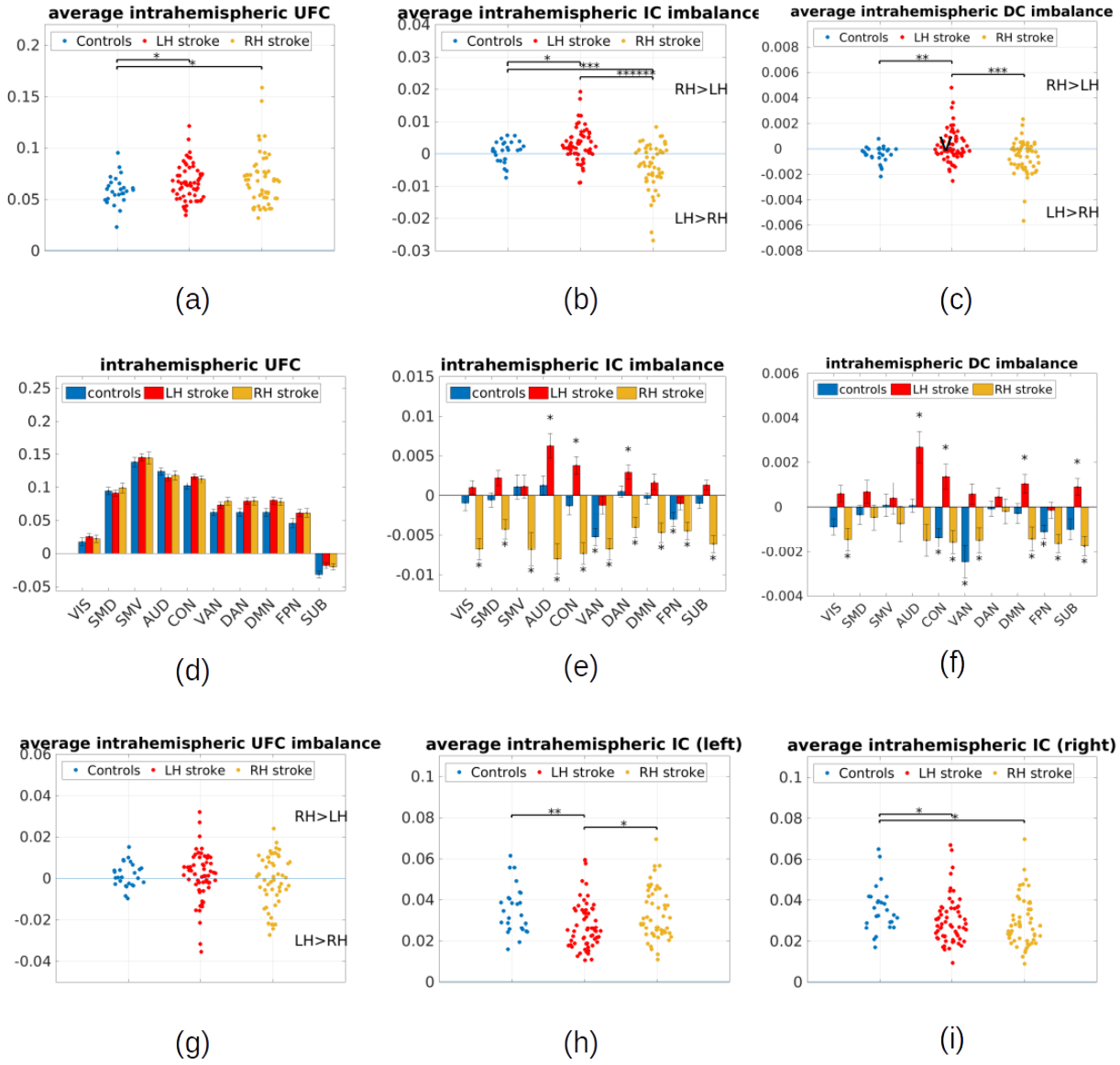

Figure 5: Average intra-hemispheric FC in acute phase. For each subject, we have computed the average intra-hemispheric UFC, IC and DC within the LH and RH hemisphere (a) the average intra-hemispheric UFC (sum of the LH and RH averages) is higher for patients than for controls. (b-c) the average imbalance (RH-LH difference) in intra-hemispheric IC and DC is positive for LH patients and negative for RH patients, implying that the average IC and DC are higher in the intact than the lesioned hemisphere (d) We show the average intra-hemispheric UFC by resting state network. Dots are averages over subjects, error bars standard errors over subjects. Stars represent networks for which comparison with controls (two-sample T-test) is not significant. (e-f) We show the imbalance in average intra-hemispheric IC, DC by resting state network. Dots are averages over subjects, error bars standard errors over subjects. Stars represent networks for which comparison with 0 (one-sample T-test) is not

significant. (g) there is no left/right imbalance in intra-hemispheric UFC for patients and controls (h) the average intra-hemispheric IC in the left hemisphere is reduced in LH patents compared to controls and RH patients (i) the average intra-hemispheric IC in the right hemisphere is reduced in RH and LH patients compared to controls. VIS=visual, SMD=sensorimotor dorsal, SMV=sensorimotor ventral, AUD=auditory network, CON=cingulo-opercular network, VAN=ventral attention network, DAN=dorsal attention network, DMN=default mode network, FPN=fronto-parietal network SUB=subcortical nodes.

Global FC and GC biomarkers and stroke-related behavioral deficits

In the previous sections, we characterized several global correlates, or biomarkers, of stroke based on functional connectivity and Granger causality analyses. Four biomarkers were related to homotopic connections: 1) UFC_{homo}: homotopic UFC; 2) IC_{homo}: homotopic IC; 3) ΣDC_{homo}: sum of homotopic DC (contralesional to ipsilesional plus ipsilesional to contralesional); 4) ΔDC_{homo}: homotopic DC asymmetry (contralesional to ipsilesional minus ipsilesional to contralesional). Both LH and RH patients, as a group, presented a reduced UFC_{homo}, a reduced IC_{homo} and an enhanced ΔDC_{homo} in comparison to healthy subjects. In addition, LH patients presented a reduction of ΣDC_{homo}. Three additional biomarkers were related to intra-hemispheric connections: 5) ΣUFC_{intra}: sum of intra-hemispheric UFC (ipsilesional plus contralesional); 6) ΔIC_{intra}: intra-hemispheric IC imbalance (contralesional minus ipsilesional); 7) ΔDC_{intra}: intra-hemispheric DC imbalance (difference of contralesional minus ipsilesional). LH and RH patients present an enhanced ΣUFC_{intra} and an enhanced ΔIC_{intra} in comparison to healthy subjects.

In order to study whether these global correlates of stroke were correlated among each other, we computed the partial Spearman correlation values between pairs of biomarkers for all patients controlling for lesion volume. Results are shown in Fig. 6a. We observed that the markers split into three groups. The first group included UFC_{homo}, IC_{homo} and ΣDC_{homo}, which were all strongly correlated. These three markers measured the strength of inter-hemispheric (homotopic) connectivity. The second group included ΔDC_{homo}, ΔIC_{intra} and ΔDC_{intra}, which were mutually correlated and uncorrelated with the homotopic measures. These three markers measured homotopic imbalance. Last, ΣUFC_{intra} was weakly correlated with the other markers. A PCA on the (z-scored) markers identified two principal components explaining 32% and 30% of the total

variance respectively (Fig. 6b), henceforth indicated as the principal components PC1 and PC2. The PC1 loaded on UFC_{homo}, IC_{homo} and ΣDC_{homo}, whereas the PC2 on ΔDC_{homo}, ΔIC_{intra} and ΔDC_{intra}. Intuitively, PC1 summarized the inter-hemispheric functional integration, PC2 the inter-hemispheric imbalance. We investigated whether PC1 and PC2 were related to the structural lesions. As shown in Fig. 6c, PC1 was negatively correlated with lesion volume (Spearman $r=-0.47$, $p<10^{-6}$): the larger the lesion, the lower the functional integration between the hemispheres (Fig. 6c). Concerning PC2, we found that the modulus of PC2 was positively correlated with lesion volume (Spearman $r=0.54$, $p<10^{-7}$): the larger the lesion, the larger the asymmetry between the hemispheres (Fig. 6d). In this regard, we should note that the value PC2 reflected the direction of the asymmetry (left-ward or right-ward), while its modulus reflected the magnitude of the asymmetry.

In a previous work (Corbetta et al., 2015), eight behavioral scores were identified, corresponding to the eight strongest principal components explaining a large fraction of variance in behavioral tests covering language, memory, motion and attention function. The eight factors were associated with language, left body motion, right body motion, spatial attention (hemispatial neglect), sustained attention, shifting attention, spatial memory, verbal memory. Higher scores were associated with better performance in each domain. Right body motion, language, verbal memory and shifting attention scores tend to be lower for LH patients, sustained attention scores show no hemispheric bias, while left body motion and spatial memory scores tend to be lower for RH patients.

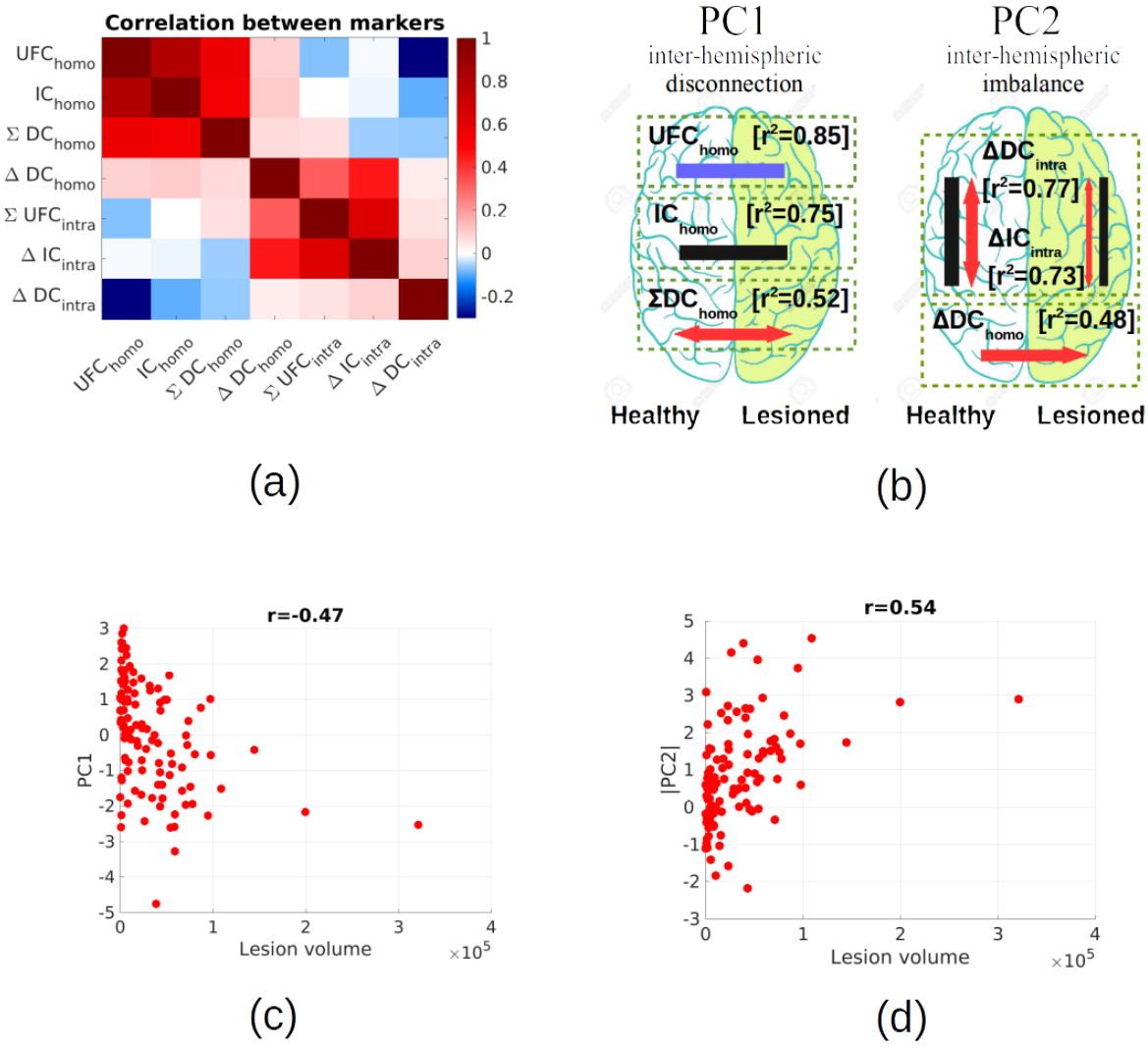

Figure 6. **Global FC and GC biomarkers.** Our analysis identified several global correlates, or biomarkers, of stroke based on functional connectivity and Granger causality analyses. (a) Looking at the correlation (partial Spearman correlation correcting for lesion volume) between each pair of markers, one can immediately notice two separate groups of correlated markers, one including UFC_{homo}, IC_{homo}, ΣDC_{homo}, the other including ΔDC_{homo} , ΔIC_{intra}, ΔDC_{intra}. (b) A PCA on the seven markers revealed two PCs explaining more than 32% and 30% of the total variance across patients. The first component (PC1) loaded on UFC_{homo}, IC_{homo}, ΣDC_{homo}, the second component (PC2) on ΔDC_{homo} , ΔIC_{intra}, ΔDC_{intra}. This is summarized in the two brain plots showing intuitively the main effects captured by PC1 and PC2 in the healthy and lesioned hemisphere. (c) PC1 correlates negatively with lesion volume (d) the modulus of PC2 correlates positively with lesion volume.

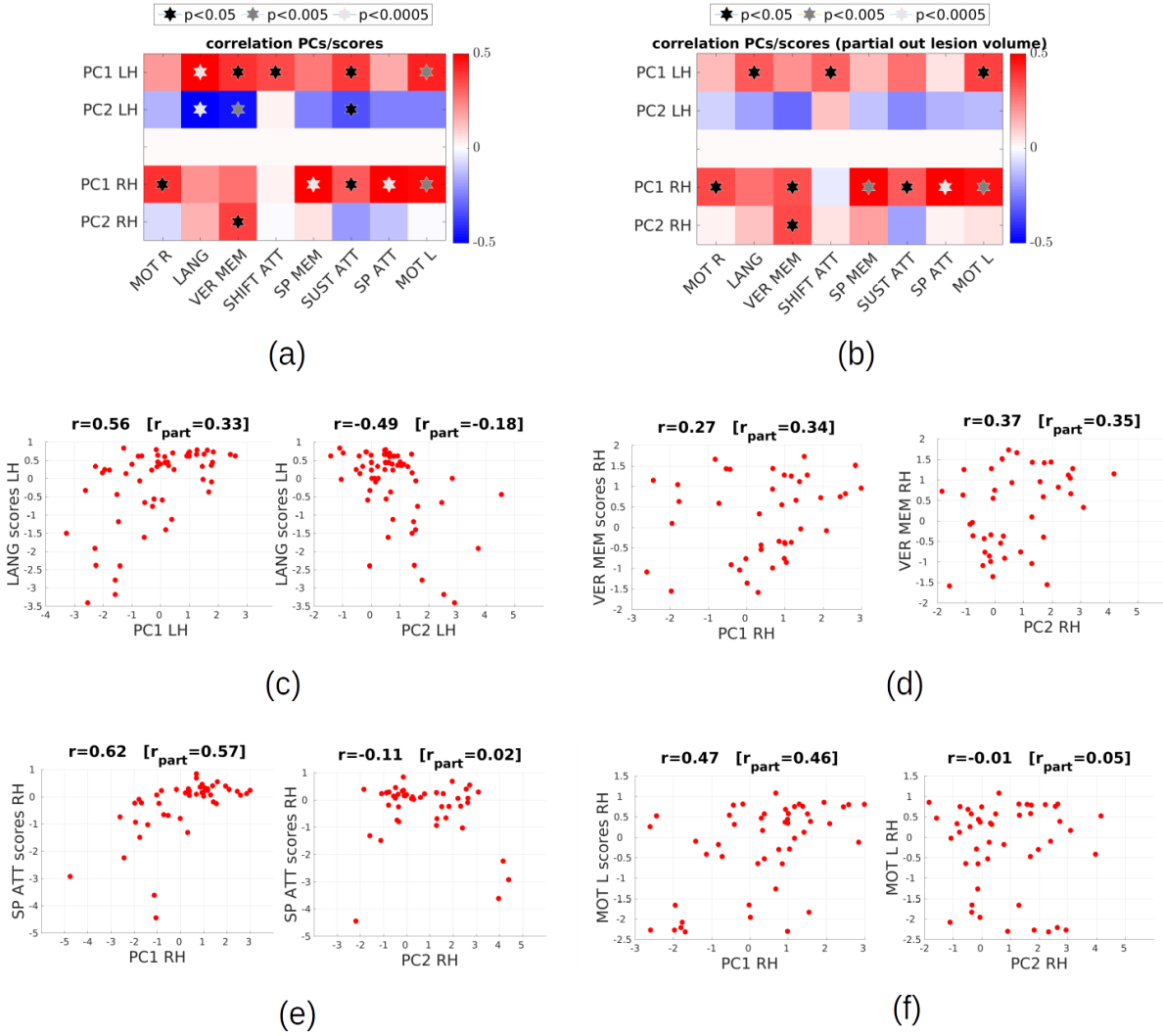

Figure 7. **Correlation with behavioral scores. :** (a) Spearman correlation between behavioral scores and the two principal components (PC) summarizing FC and GC stroke markers (b) partial Spearman correlation between behavioral scores and the two principal components, correcting for lesion volume (c) scatter plot of PC1/PC2 versus language scores for LH patients (d) scatter plot of PC1/PC2 vs verbal memory scores for RH patients (e) scatter plot of PC1/PC2 vs spatial attention scores for RH patients (f) scatter plot of PC1/PC2 versus left body motion scores for RH patients

We quantified to which extent the first two principal components (PC1 and PC2) were predictive of the observed behavioral deficits. To do so, we computed the Spearman correlation between the two PCs and behavioral scores (Fig. 7a). We had two general predictions. First, we expected a positive correlation between performance and inter-hemispheric integration (Carter 2010, Siegel 2016, Corbetta 2018). Consequently, we expected PC1 to correlate positively with behavioral scores. Second, we expected that a decrease of connectivity within and from the lesioned hemisphere would have been generally detrimental for performance. Hence, behavioral scores were expected to correlate negatively with PC2. These expectations were partially met. PC1 correlated positively with all scores for both LH and RH, in agreement with expectation. PC2 correlated negatively for LH patients, while correlations were weaker and ambiguous in sign for RH patients. Since PC1 and PC2 correlate with lesion volume, part of the observed correlation with behavioral scores may be explained by lesion volume. Therefore, we computed the partial Spearman correlation between the two PCs and behavioral scores, controlling for the effect of lesion volume (Fig. 7b). While results are qualitatively similar, correlations are weaker, especially for LH patients.

Concerning language and verbal memory scores, we observed a significant positive correlation with PC1 and a negative correlation with PC2 for LH patients (Fig. 7c, 7d). These correlations, however, were mostly explained by lesion volume. For RH patients, whose language ability was less affected by the lesion, both PC1 and PC2 correlated positively with scores (significantly for verbal memory), even after controlling for lesion volume. This result suggests a supportive role of the contralesional (language-dominant) left hemisphere in the case of right lesions. Concerning attentional deficits, previous literature suggests that higher scores are associated with a higher inter-hemispheric integration, as well as a higher intra-hemispheric integration in the lesioned hemisphere (Corbetta et al. 2005, He et al. 2007, Corbetta and Shulman 2011). Consistently with this picture, we found a significant positive correlation with PC1, and a negative correlation with PC2 for sustained attention scores. However, a large part of the correlation was explained by lesion volume. For spatial attention, the

same qualitative behavior was found, but the only significant correlation occurred between PC1 and spatial attention scores for RH patients, highlighting a relevant role of inter-hemispheric integration for (RH-dominant) neglect (Fig. 7e). For shifting-attention scores, we found weak correlations (except between PC1 and shifting attention scores for LH patients). Finally, for what concerns motor deficits, previous literature (Carter et al., 2010; Siegel et al., 2016) showed that higher performance was associated with higher inter-hemispheric integration. Indeed, we found that right- and left-body motion scores correlated positively with PC1. Surprisingly, while the correlation between (right-hemisphere-controlled) left body motion and PC1 was significant for RH patients, even after partialling out lesion volume (Fig. 7f), the correlation between (left-hemisphere-controlled) right body motion and PC1 was not significant for LH patients. This suggests that right motor function (based in the left hemisphere) depends less on interaction with the contralateral hemisphere than right motor function (based in the left hemisphere). Moreover, motor scores correlated negatively, but weakly (non-significant values) with PC2.

Control analyses for potential confounds

We finally performed control analyses to investigate potential confounding effects associated with nuisance sources and hemodynamic lags. GC analyses were performed on preprocessed BOLD signals without global signal regression (GSR) removal. The rationale for this choice was that GSR may effectively work as a “temporal filter” (Liu et al., 2017, Nalci et al., 2019), suppressing the contribution of time points associated with low global signal, potentially distorting the estimation of information flows in GC. While standardly adopted for UFC estimation, GSR is a contentious step (Saad et al., 2012), particularly when one compares healthy subjects with neurological or psychiatric patients (Hahamy et al., 2014; Yang et al., 2014). Indeed, the global signal can reflect extended correlation of neural origin (Schölvinck et al., 2010), possibly differing between patients and control subjects. By applying GSR our data, homotopic information transfer (homotopic IC and bidirectional DC) presented similar effects to those found without GSR, including the asymmetry in homotopic DC (Fig. 8a). However, results on intra-hemispheric GC differed: no clear imbalance is observed in

intra-hemispheric DC or IC (Fig. 8b and 8c). Thus, GSR significantly attenuates the hemispheric imbalances. However, due to the high network specificity of the observed imbalances, it appears unlikely that such imbalances represent metabolic, movement, breathing-rate, cardiovascular or vigilance effects. It is more likely that differences in global signal between the hemispheres represent alterations in the excitation/inhibition balance within each hemisphere (Yang et al., 2014), which are obscured by GSR.

Hemodynamic lags represent an additional potential confound for our results. In fact, stroke can cause a pathologic delay in the hemodynamic response in the perilesional area, or in a wider area subserved by the occluded artery (Siegel et al., 2016b). This delay may introduce spurious “lags” of non-neural origin between regions in this area and homologous regions in the intact hemisphere, thus contributing to the observed homotopic DC asymmetry. We checked that the observed global homotopic DC asymmetry did not originate from asymmetries in the perilesional area. We considered each region *X* in the lesioned hemisphere and computed the DC asymmetry $G_{Y\to X} = F_{Y\to X} - F_{X\to Y}$ where *Y* is the homologous area in the intact hemisphere. We thus obtained brain-wide maps of homotopic DC asymmetry that we could overlay with the lesion maps (to produce the homotopic DC maps, we assigned the value $G_{Y\to X}$ to all voxels within a radius of 10mm around the center of each ROI *X*, and then applied 10mm Gaussian smoothing). In Fig. 8d, we show the results for a representative subject.The strongest DC asymmetries were observed far from the lesions location in the brain. In order to have a more quantitative control, we repeated our analyses excluding all regions at a distance less than 4cm from the lesioned area. As shown in Fig. 8e-8g, the homotopic DC asymmetry is still present after this removal, while the intra-hemispheric IC and DC imbalance appear to be even strengthened. This showed that the observed effects are not due to anomalous hemodynamic lags in the vicinity of the lesion.

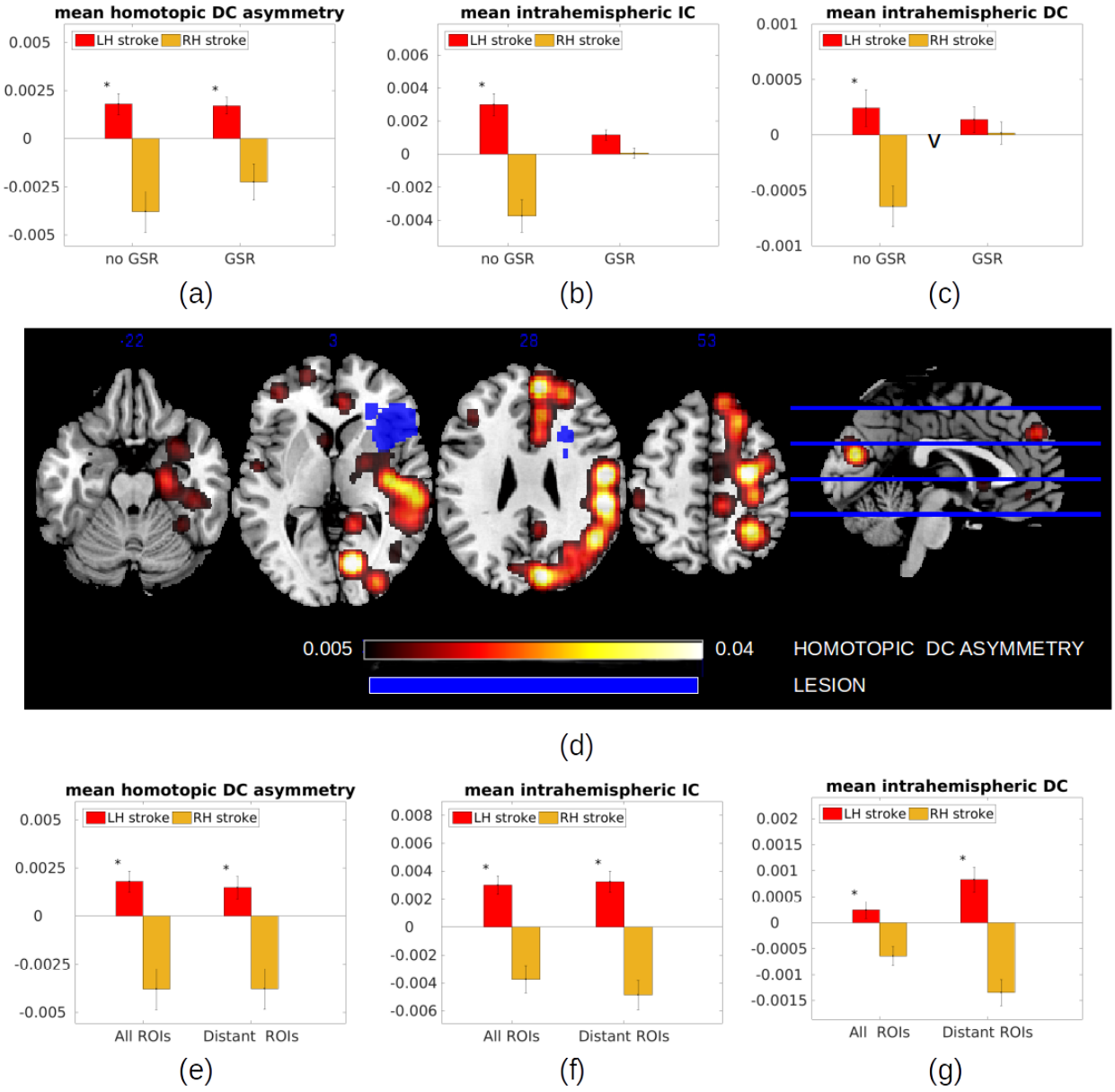

Figure 8. Control for possible confounds. (a-c) We checked the effect of GSR on the found inter-hemispheric imbalances. GSR has no effect on the homotopic DC asymmetry, while it removes the imbalance in intra-hemispheric IC and DC. (d-g) We checked possible influences of perilesional hemodynamic anomalies on our results. In (d) we verified whether the homotopic DC asymmetry could be driven by hemodynamic lags in the perilesional area. We show a map of the homotopic DC asymmetry for one representative subject, together with the lesion location (in blue). Strongest homotopic DC asymmetries are found far from the lesion. In (e-g) we show the effect of removing from analysis all regions at a distance < 4cm from the lesion. Such removal has no effect on the homotopic DC asymmetry, while it strengthens the imbalance observed in intra-hemispheric IC and DC.

DISCUSSION

Stroke-related modulations in inter- and intra-hemispheric coupling revealed by Granger causality analyses

In agreement with previous research (Corbetta et al., 2018; Golestani et al., 2013; Joshua Sarfaty Siegel et al., 2016; Tang et al., 2016), we observed that stroke produces a significant decrease in inter-hemispheric UFC, particularly for homotopic connections (Fig. 3a). One of the simplest explanations is that damage to structural connectivity between the hemispheres causes a reduction of inter-hemispheric interaction, leading to a decrease in UFC. Inter-hemispheric structural connectivity is chiefly supported by homotopic connections crossing the corpus callosum (Schmahmann et al., 2009). Experiments show that when the callosum is severed, a strong suppression of inter-hemispheric FC occurs (Mancuso et al., 2019; Roland et al., 2017; O'Reilly et al., 2013), in agreement with *in silico* modeling showing that the removal of structural homotopic connections produces a nearly complete loss of inter-hemispheric FC (Messé et al., 2014). In fact, recent work showed that inter-hemispheric structural connectivity is damaged in stroke, and that patterns of structural disconnection correlate with UFC alterations (Griffis et al., 2019, Griffis et al., 2020).

Our results from GC-based analyses support the hypothesis that the UFC decrease is associated with a loss of inter-hemispheric interaction. Indeed, homotopic IC and DC, which together quantify inter-hemispheric information transfer, showed a consistent decrease in stroke patients (Fig. 4b, 4c). The severity of the decrease correlated with lesion volume. The IC captured zero-lag ("instantaneous") cortico-cortical interactions occurring within 1 TR, while DC captured lagged cortico-cortical interactions occurring on a time scale longer than 1 TR. Classically, IC are interpreted as originating from external common inputs (Ding et al., 2006). Our results, therefore, suggest that a component of stroke-related alterations in cortico-cortical coupling emerges from disrupted common inputs, potentially from regions that project symmetrically to cortical areas, such as subcortical structures. This hypothesis is supported by structural analyses that locate stroke lesions primarily in subcortical areas, such as the thalamus (Corbetta et al. 2015), as well as by recent experimental work showing that subcortical

structures can play a large role in maintaining FC between cortical regions when direct influences are impaired (Canella et al. 2020). However, given the slow sampling rate of fMRI (TR=2s), an IC decrease cannot be uniquely attributed to a loss of common input, as it may also result from a decrease of fast directed interactions occurring on timescale shorter than 2s. To which extent subcortical structures contribute in re-modulating cortical interaction remains a relevant topic for further investigation.

Our results on homotopic DC showed that stroke impacts the inter-hemispheric information flow asymmetrically, with a spared information flow from the healthy to the lesioned hemisphere (Fig. 4a). Such effect hints at an asymmetry in the strength of inter-hemispheric communication. This asymmetric effect is not immediately explained by structural lesions, since there is no evidence that ischemia would affect selectively fibers from the ipsilesional to the contralesional hemisphere rather than in the opposite direction.

However, our analysis of intra-hemispheric GC also revealed a functional imbalance between the hemispheres in stroke patients, characterized by higher intra-hemispheric IC and DC in the intact hemisphere than in the lesioned one (Fig. 5b and 5c). Our results are not conclusive regarding the relation between the homotopic DC asymmetry (Fig. 4a) and the imbalance in intra-hemispheric IC and DC. However, we provided evidence that the intra-hemispheric and inter-hemispheric imbalances are correlated (Fig. 6), which suggests that the two results are not independent and may have a common cause. We hypothesize that both effects could stem from a hypoactivity of the lesioned hemisphere due to a loss of inter-areal excitatory influences. In models of spontaneous whole-brain activity (Kringelbach and Deco, 2019), the excitatory influence one region exerts onto another is determined by the amount of structural connections between the two, and the level of activity of the first region. Since stroke can damage structural connections between ipsilesional areas, we could generally expect a loss of excitatory influences, and hence general activity decrease, within the lesioned hemisphere (Grefkes and Fink, 2014). This, in turn, would also imply that the lesioned hemisphere would exert less excitation on the healthy one. This picture would explain both the decrease of ipsilesional DC and IC, and the decrease of DC from the lesioned to the healthy hemisphere. Moreover, such interpretation supported by the fact that all

imbalance measures (ΔDC_{homo}, ΔIC_{intra}, ΔDC_{intra}) correlate negatively with lesion volume (i.e., the stronger the lesion, the higher the intra- and inter-hemispheric functional imbalances).

Post-stroke inter-hemispheric imbalances in effective connectivity were widely reported in the motor system, as reviewed in (Grefkes and Fink, 2014). During motor tasks, excitatory influences within the lesioned hemisphere are reduced, contributing to a general decrease of ipsilesional brain activity (Grefkes and Fink, 2014; Rehme and Grefkes, 2013). Congruently, stimulating the lesioned hemisphere can promote better recovery (Takeuchi and Izumi, 2012). As for inter-hemispheric connectivity, several studies on the motor system after stroke indicate an anomalous influence of the contralesional hemisphere onto the lesioned one during motor tasks (Rehme and Grefkes, 2013, Grefkes et al., 2010, Grefkes and Fink, 2014). Whether the contralesional influence is inhibitory (hence detrimental to motor performance), or excitatory (hence supportive of performance) seems to depend on several factors, including time after stroke and severity of the lesions (Pino et al., 2014). Our results instead showed a decrease of influence of the damaged hemisphere on the normal one. However, we are wary of a direct comparison, since our whole-brain results were obtained with a resting-state paradigm, hence without any specific involvement of the motor cortex. In order to further clarify inter-hemispheric balance after stroke, future whole-brain studies should discriminate between excitatory and inhibitory influences, which is not possible in the current GC analysis.

Hemispheric functional imbalance and stroke-related behavioral deficits

Our results highlight functional and behavioral differences depending on which hemisphere is lesioned. Previous work on this cohort (Corbetta et al., 2015; Ramsey et al., 2017) identified sets of correlated deficits for left and right lesions respectively, largely agreeing with hemispheric functional asymmetries maps described in healthy subjects (Karolis et al., 2019). In LH patients, we observed that the decrease of inter-hemispheric communication (summarized by PC1) correlated with behavior for domains that are specific to the left hemisphere (language, verbal memory, attention shifting) or both hemispheres (sustained attention). Conversely, in RH patients PC1

correlated with behavior for domains more associated with the right hemisphere (motor function, spatial and sustained attention, and spatial memory). For LH patients the correlation was significantly lower if lesion volume was regressed, and presently we cannot discriminate the specific impact of inter-hemispheric communication loss on behavioral function from other possible effects resulting from the lesion. However, in RH patients correlations were more robust to regression of lesion volume, which suggests a specific impact of inter-hemispheric communication loss. This agrees with previous studies showing that deficits that were affected by right lesions, such as spatial attention deficits, were more associated with inter-hemispheric rather than intra-hemispheric functional disconnection (Baldassarre et al., 2016a, 2016b; Siegel et al., 2016). We speculate that input from the LH may be more critical for functional integrity of the RH than the other way around, congruently with studies reporting that the left hemisphere presents more central or indispensable regions for the whole-brain structural network (Iturria-Medina et al., 2011), and that the right hemisphere depends more heavily on integration with the left one than the other way around (Gotts et al., 2013). Also congruent with this hypothesis would be the fact that left lesions induce a symmetrical effect (bilateral reduction of intra-hemispheric DC, and a bidirectional reduction of homotopic DC), while right lesions have a more lateralized effect (decrease of intra-hemispheric DC in the right hemisphere, and homotopic DC from the RH to the LH). Concerning the imbalance between the hemispheres, summarized by PC2, we also observe a difference between left and right hemisphere patients. In LH patients PC2 correlated negatively with behavioral scores, while such effect was absent in RH patients (except for verbal memory, for which the imbalance impacts positively on scores). The negative correlation between PC2 and behavioral scores of LH patients was significant for behaviors that were affected by left hemisphere lesions (language, verbal memory) and could be largely explained by lesion volume, suggesting that it reflects the extent of intra-hemispheric LH damage. Instead, for RH patients we did not observe such correlation, suggesting that intra-hemispheric damage has a lesser impact on behavior. Instead, the positive correlation between PC2 and verbal memory scores suggests a supportive role of the left (contralesional) hemisphere for a left-lateralized function in the case of right lesions.

Methodological considerations on Granger causality analyses: advantages and limitations

The efficacy of GC as a data-driven analysis method rests on its ability to uncover global patterns of information flow and differences in information flows between groups or experimental conditions in a completely unsupervised way (Faes et al., 2017; Friston et al., 2013; Roebroeck et al., 2011, 2005). Our results show that whole-brain covariance-based GC analysis is well-suited to characterize group differences in inter-areal directional interactions from resting state fMRI, provided that the correct lag *L* is estimated from the data and used for the analyses. The main limitation of our analysis is the uncertainty affecting individual GC estimates (Fig. 2). For each GC-based stroke marker (e.g., the total homotopic IC), we obtained a large group variance, and consequently a large overlap between the distributions of patients and controls, so that we could not robustly classify an individual as patient or control based on his/her value of the marker. It is likely that part of this variance reflects estimation error, rather than true interindividual variability. Analogously, the uncertainty affecting single-subject estimates also implies a difficulty in relating individual GC results with individual behavioral scores. Thus, estimation error limits the use of GC for the development of personalized biomarkers predictive of clinical condition and behavioral performance at the single-patient level. This limitation is not inherent in GC per se, but depends on the relative paucity of functional data available for each patient. By taking longer recordings or repeating recording sessions, we could obtain much more accurate GC estimates. Improved GC estimates may also be obtained by using a lower TR (TR=0.6s would more than triple the number of points for estimation, besides offering improved time resolution and a better artifact detection). Finally, improved GC estimates may be obtained by adopting a different, more computationally intensive framework for GC estimation. For instance, a possible way to improve GC estimates would be to harness the potentially useful information contained in single-voxel time courses, performing a multivariate GC analysis on pairs of voxels within the two regions as in Tang et al. 2012. To avoid computational problems associated with the large number of nodes, one may focus analysis on specific links (e.g., homotopic links) revealing large controls/patient differences in the covariance-based analyses.

Conclusions

To conclude, the Granger causality (GC) analysis of inter-areal interactions after stroke highlighted two broad pathological features. First, a decrease of homotopic GC, suggesting a large decrease of interhemispheric communication, either direct or mediated by subcortical structures. Second, an inter-hemispheric imbalance, revealed by an asymmetry in homotopic GC, as well as a right-left difference in intra-hemispheric GC, suggesting a decrease of communication within and from the lesioned hemisphere. These results show that previously observed FC alterations in stroke are related to broad changes in inter-areal communication. Furthermore, our analysis confirms and generalizes previous findings about post-stroke inter-hemispheric imbalances in the motor and attention system. Both of the observed GC anomalies were related to behavioral deficits. The global decrease in inter-hemispheric communication was highly detrimental to behavioral performance in all domains, while the inter-hemispheric imbalance was generally detrimental only for patients with left hemisphere lesions, with more domain-specific effects. This finding indicates that the role of the contralesional hemisphere may be supportive or detrimental depending on the lesioned hemisphere, and the specific cognitive function. Overall, our results show the usefulness of whole-brain GC analysis to uncover pathological anomalies in inter-areal communication, and may boost the development of whole-brain models that reproduce large-scale interareal communication patterns, as well as the design of stimulation therapies aimed at improving recovery.

REFERENCES

Baldassarre, A., Ramsey, L., Hacker, C.L., Callejas, A., Astafiev, S.V., Metcalf, N.V., Zinn, K., Rengachary, J., Snyder, A.Z., Carter, A.R., Shulman, G.L., Corbetta, M., 2014. Large-scale changes in network interactions as a physiological signature of spatial neglect. Brain 137, 3267–3283. https://doi.org/10.1093/brain/awu297

Barnett, L., Barrett, A.B., Seth, A.K., 2009. Granger Causality and Transfer Entropy Are Equivalent for Gaussian Variables. Phys. Rev. Lett. 103, 238701. https://doi.org/10.1103/PhysRevLett.103.238701

Barnett, L., Seth, A.K., 2014. The MVGC multivariate Granger causality toolbox: A new approach to Granger-causal inference. J. Neurosci. Methods 223, 50–68. https://doi.org/10.1016/j.jneumeth.2013.10.018

Beirlant, J., Dudewicz, E.J., Györfi, L., Van der Meulen, E.C., 1997. Nonparametric entropy estimation: An overview. Int. J. Math. Stat. Sci. 6, 17–39.

Brovelli, A., Chicharro, D., Badier, J.-M., Wang, H., Jirsa, V., 2015. Characterization of Cortical Networks and Corticocortical Functional Connectivity Mediating Arbitrary Visuomotor Mapping. J. Neurosci. 35, 12643–12658. https://doi.org/10.1523/JNEUROSCI.4892-14.2015

Bullmore, E., Sporns, O., 2009. Complex brain networks: graph theoretical analysis of structural and functional systems. Nat. Rev. Neurosci. 10, 186–198. https://doi.org/10.1038/nrn2575

Canella, C., Rocchi, F., Noei, S., Gutierrez-Barragan, D., Coletta, L., Galbusera, A., ... & Gozzi, A. (2020). Cortical silencing results in paradoxical fMRI overconnectivity. *bioRxiv*.

Carter, A.R., Astafiev, S.V., Lang, C.E., Connor, L.T., Rengachary, J., Strube, M.J., Pope, D.L.W., Shulman, G.L., Corbetta, M., 2010. Resting interhemispheric functional magnetic resonance imaging connectivity predicts performance after stroke. Ann. Neurol. 67, 365–375. https://doi.org/10.1002/ana.21905

Chicharro, D., Ledberg, A., 2012. Framework to study dynamic dependencies in networks of interacting processes. Phys. Rev. E 86, 041901. https://doi.org/10.1103/PhysRevE.86.041901

Corbetta, Maurizio, et al. "Neural basis and recovery of spatial attention deficits in spatial neglect." *Nature neuroscience* 8.11 (2005): 1603-1610. https://www.nature.com/articles/nn1574

Corbetta, Maurizio, and Gordon L. Shulman. "Spatial neglect and attention networks." *Annual review of neuroscience* 34 (2011): 569-599.

https://www.annualreviews.org/doi/pdf/10.1146/annurev-neuro-061010-113731

Corbetta, M., Ramsey, L., Callejas, A., Baldassarre, A., Hacker, C.D., Siegel, J.S., Astafiev, S.V., Rengachary, J., Zinn, K., Lang, C.E., Connor, L.T., Fucetola, R., Strube, M., Carter, A.R., Shulman, G.L., 2015. Common Behavioral Clusters and Subcortical Anatomy in Stroke. Neuron 85, 927–941. https://doi.org/10.1016/j.neuron.2015.02.027

Corbetta, M., Siegel, J.S., Shulman, G.L., 2018. On the low dimensionality of behavioral deficits and alterations of brain network connectivity after focal injury. Cortex, In Memory of Professor Glyn Humphreys 107, 229–237. https://doi.org/10.1016/j.cortex.2017.12.017

Damoiseaux, J.S., Rombouts, S. a. R.B., Barkhof, F., Scheltens, P., Stam, C.J., Smith, S.M., Beckmann, C.F., 2006. Consistent resting-state networks across healthy subjects. Proc. Natl. Acad. Sci. 103, 13848–13853. https://doi.org/10.1073/pnas.0601417103

Eldaief, M.C., McMains, S., Hutchison, R.M., Halko, M.A., Pascual-Leone, A., 2017. Reconfiguration of Intrinsic Functional Coupling Patterns Following Circumscribed Network Lesions. Cereb. Cortex 27, 2894–2910. https://doi.org/10.1093/cercor/bhw139

Faes, L., Stramaglia, S., Marinazzo, D., 2017. On the interpretability and computational reliability of frequency-domain Granger causality. F1000Research 6. https://doi.org/10.12688/f1000research.12694.1

Fox, M.D., Snyder, A.Z., Vincent, J.L., Corbetta, M., Essen, D.C.V., Raichle, M.E., 2005. The human brain is intrinsically organized into dynamic, anticorrelated functional networks. Proc. Natl. Acad. Sci. 102, 9673–9678. https://doi.org/10.1073/pnas.0504136102

Friston, K., Moran, R., Seth, A.K., 2013. Analysing connectivity with Granger causality and dynamic causal modelling. Curr. Opin. Neurobiol., Macrocircuits 23, 172–178. https://doi.org/10.1016/j.conb.2012.11.010

Geschwind, N., Galaburda, A.M., 1985. Cerebral Lateralization: Biological Mechanisms, Associations, and Pathology: I. A Hypothesis and a Program for Research. Arch. Neurol. 42, 428–459. https://doi.org/10.1001/archneur.1985.04060050026008

Geweke, J., 1982. Measurement of Linear Dependence and Feedback between Multiple Time Series. J. Am. Stat. Assoc. 77, 304–313. https://doi.org/10.1080/01621459.1982.10477803

Golestani, A.-M., Tymchuk, S., Demchuk, A., Goodyear, B.G., 2013. Longitudinal Evaluation of Resting-State fMRI After Acute Stroke With Hemiparesis. Neurorehabil. Neural Repair 27, 153–163. https://doi.org/10.1177/1545968312457827

Gordon, E.M., Laumann, T.O., Adeyemo, B., Huckins, J.F., Kelley, W.M., Petersen, S.E., 2016. Generation and Evaluation of a Cortical Area Parcellation from Resting-State

Correlations. Cereb. Cortex 26, 288–303. https://doi.org/10.1093/cercor/bhu239

Gotts, S.J., Jo, H.J., Wallace, G.L., Saad, Z.S., Cox, R.W., Martin, A., 2013. Two distinct forms of functional lateralization in the human brain. Proc. Natl. Acad. Sci. 110, E3435–E3444. https://doi.org/10.1073/pnas.1302581110

Granger, C.W.J., 1969. Investigating Causal Relations by Econometric Models and Cross-spectral Methods. Econometrica 37, 424–438. https://doi.org/10.2307/1912791

Gratton, C., Nomura, E.M., Pérez, F., D'Esposito, M., 2012. Focal Brain Lesions to Critical Locations Cause Widespread Disruption of the Modular Organization of the Brain. J. Cogn. Neurosci. 24, 1275–1285. https://doi.org/10.1162/jocn_a_00222

Grefkes, C., Fink, G.R., 2014. Connectivity-based approaches in stroke and recovery of function. Lancet Neurol. 13, 206–216. https://doi.org/10.1016/S1474-4422(13)70264-3

Griffis, J.C., Metcalf, N.V., Corbetta, M., Shulman, G.L., 2020. Damage to the shortest structural paths between brain regions is associated with disruptions of resting-state functional connectivity after stroke. NeuroImage 210, 116589. https://doi.org/10.1016/j.neuroimage.2020.116589

Griffis, J.C., Metcalf, N.V., Corbetta, M., Shulman, G.L., 2019. Structural Disconnections Explain Brain Network Dysfunction after Stroke. Cell Rep. 28, 2527-2540.e9. https://doi.org/10.1016/j.celrep.2019.07.100

Hahamy, A., Calhoun, V., Pearlson, G., Harel, M., Stern, N., Attar, F., Malach, R., Salomon, R., 2014. Save the Global: Global Signal Connectivity as a Tool for Studying Clinical Populations with Functional Magnetic Resonance Imaging. Brain Connect. 4, 395–403. https://doi.org/10.1089/brain.2014.0244

He, B.J., Snyder, A.Z., Vincent, J.L., Epstein, A., Shulman, G.L., Corbetta, M., 2007. Breakdown of Functional Connectivity in Frontoparietal Networks Underlies Behavioral Deficits in Spatial Neglect. Neuron 53, 905–918. https://doi.org/10.1016/j.neuron.2007.02.013

Hlinka, J., Paluš, M., Vejmelka, M., Mantini, D., Corbetta, M., 2011. Functional connectivity in resting-state fMRI: Is linear correlation sufficient? NeuroImage 54, 2218–2225. https://doi.org/10.1016/j.neuroimage.2010.08.042

Ince, R.A.A., Giordano, B.L., Kayser, C., Rousselet, G.A., Gross, J., Schyns, P.G., 2017. A statistical framework for neuroimaging data analysis based on mutual information estimated via a gaussian copula. Hum. Brain Mapp. 38, 1541–1573. https://doi.org/10.1002/hbm.23471

Iturria-Medina, Y., Pérez Fernández, A., Morris, D.M., Canales-Rodríguez, E.J., Haroon, H.A., García Pentón, L., Augath, M., Galán García, L., Logothetis, N., Parker, G.J.M.,

Melie-García, L., 2011. Brain Hemispheric Structural Efficiency and Interconnectivity Rightward Asymmetry in Human and Nonhuman Primates. Cereb. Cortex 21, 56–67. https://doi.org/10.1093/cercor/bhq058

Josse, Goulven, and Nathalie Tzourio-Mazoyer. "Hemispheric specialization for language." *Brain Research Reviews* 44.1 (2004): 1-12.

Karolis, V.R., Corbetta, M., Thiebaut de Schotten, M., 2019. The architecture of functional lateralisation and its relationship to callosal connectivity in the human brain. Nat. Commun. 10, 1417. https://doi.org/10.1038/s41467-019-09344-1

Kringelbach, M.L., Deco, G., 2019. 24 - Whole-brain modeling of neuroimaging data: Moving beyond correlation to causation, in: Raz, A., Thibault, R.T. (Eds.), Casting Light on the Dark Side of Brain Imaging. Academic Press, pp. 139–143. https://doi.org/10.1016/B978-0-12-816179-1.00024-4

Liu, T.T., Nalci, A., Falahpour, M., 2017. The global signal in fMRI: Nuisance or Information? NeuroImage 150, 213–229. https://doi.org/10.1016/j.neuroimage.2017.02.036

Mancuso, L., Uddin, L.Q., Nani, A., Costa, T., Cauda, F., 2019. Brain functional connectivity in individuals with callosotomy and agenesis of the corpus callosum: A systematic review. Neurosci. Biobehav. Rev. 105, 231–248. https://doi.org/10.1016/j.neubiorev.2019.07.004

Marko, H., 1973. The Bidirectional Communication Theory - A Generalization of Information Theory. IEEE Trans. Commun. 21, 1345–1351. https://doi.org/10.1109/TCOM.1973.1091610

McQuarrie, A.D.R., Tsai, C.-L., 1998. Regression and Time Series Model Selection. World Scientific.

Melozzi, F., Bergmann, E., Harris, J.A., Kahn, I., Jirsa, V., Bernard, C., 2019. Individual structural features constrain the mouse functional connectome. Proc. Natl. Acad. Sci. 116, 26961–26969. https://doi.org/10.1073/pnas.1906694116

Mengotti, Paola, et al. "Lateralization, functional specialization, and dysfunction of attentional networks." *Cortex* (2020).

Messé, A., Rudrauf, D., Benali, H., Marrelec, G., 2014. Relating Structure and Function in the Human Brain: Relative Contributions of Anatomy, Stationary Dynamics, and Non-stationarities. PLoS Comput. Biol. 10. https://doi.org/10.1371/journal.pcbi.1003530

New, A.B., Robin, D.A., Parkinson, A.L., Duffy, J.R., McNeil, M.R., Piguet, O., Hornberger, M., Price, C.J., Eickhoff, S.B., Ballard, K.J., 2015. Altered resting-state network connectivity in stroke patients with and without apraxia of speech. NeuroImage Clin. 8, 429–439. https://doi.org/10.1016/j.nicl.2015.03.013

O'Reilly, J.X., Croxson, P.L., Jbabdi, S., Sallet, J., Noonan, M.P., Mars, R.B., Browning, P.G.F., Wilson, C.R.E., Mitchell, A.S., Miller, K.L., Rushworth, M.F.S., Baxter, M.G., 2013. Causal effect of disconnection lesions on interhemispheric functional connectivity in rhesus monkeys. Proc. Natl. Acad. Sci. 110, 13982–13987. https://doi.org/10.1073/pnas.1305062110

Park Chang-hyun, Chang Won Hyuk, Ohn Suk Hoon, Kim Sung Tae, Bang Oh Young, Pascual-Leone Alvaro, Kim Yun-Hee, 2011. Longitudinal Changes of Resting-State Functional Connectivity During Motor Recovery After Stroke. Stroke 42, 1357–1362. https://doi.org/10.1161/STROKEAHA.110.596155

Pino, G.D., Pellegrino, G., Assenza, G., Capone, F., Ferreri, F., Formica, D., Ranieri, F., Tombini, M., Ziemann, U., Rothwell, J.C., Lazzaro, V.D., 2014. Modulation of brain plasticity in stroke: a novel model for neurorehabilitation. Nat. Rev. Neurol. 10, 597–608. https://doi.org/10.1038/nrneurol.2014.162

Ramsey, L.E., Siegel, J.S., Baldassarre, A., Metcalf, N.V., Zinn, K., Shulman, G.L., Corbetta, M., 2016. Normalization of network connectivity in hemispatial neglect recovery. Ann. Neurol. 80, 127–141. https://doi.org/10.1002/ana.24690

Rehme, A.K., Grefkes, C., 2013. Cerebral network disorders after stroke: evidence from imaging-based connectivity analyses of active and resting brain states in humans. J. Physiol. 591, 17–31. https://doi.org/10.1113/jphysiol.2012.243469

Rissanen, J., Wax, M., 1987. Measures of mutual and causal dependence between two time series (Corresp.). IEEE Trans. Inf. Theory 33, 598–601. https://doi.org/10.1109/TIT.1987.1057325

Roebroeck, A., Formisano, E., Goebel, R., 2011. The identification of interacting networks in the brain using fMRI: Model selection, causality and deconvolution. NeuroImage 58, 296–302. https://doi.org/10.1016/j.neuroimage.2009.09.036

Roebroeck, A., Formisano, E., Goebel, R., 2005. Mapping directed influence over the brain using Granger causality and fMRI. NeuroImage 25, 230–242. https://doi.org/10.1016/j.neuroimage.2004.11.017

Roland, J.L., Snyder, A.Z., Hacker, C.D., Mitra, A., Shimony, J.S., Limbrick, D.D., Raichle, M.E., Smyth, M.D., Leuthardt, E.C., 2017. On the role of the corpus callosum in interhemispheric functional connectivity in humans. Proc. Natl. Acad. Sci. 114, 13278–13283. https://doi.org/10.1073/pnas.1707050114

Saad, Z.S., Gotts, S.J., Murphy, K., Chen, G., Jo, H.J., Martin, A., Cox, R.W., 2012. Trouble at Rest: How Correlation Patterns and Group Differences Become Distorted After Global

Signal Regression. Brain Connect. 2, 25–32. https://doi.org/10.1089/brain.2012.0080

Schmahmann, J.D., Schmahmann, J., Pandya, D., 2009. Fiber Pathways of the Brain. Oxford University Press, USA.

Schölvinck, M.L., Maier, A., Ye, F.Q., Duyn, J.H., Leopold, D.A., 2010. Neural basis of global resting-state fMRI activity. Proc. Natl. Acad. Sci. 107, 10238–10243. https://doi.org/10.1073/pnas.0913110107

Schreiber, T., 2000. Measuring Information Transfer. Phys. Rev. Lett. 85, 461–464. https://doi.org/10.1103/PhysRevLett.85.461

Siegel, Joshua Sarfaty, Ramsey, L.E., Snyder, A.Z., Metcalf, N.V., Chacko, R.V., Weinberger, K., Baldassarre, A., Hacker, C.D., Shulman, G.L., Corbetta, M., 2016. Disruptions of network connectivity predict impairment in multiple behavioral domains after stroke. Proc. Natl. Acad. Sci. 113, E4367–E4376. https://doi.org/10.1073/pnas.1521083113

Siegel, Joshua S, Snyder, A.Z., Ramsey, L., Shulman, G.L., Corbetta, M., 2016. The effects of hemodynamic lag on functional connectivity and behavior after stroke. J. Cereb. Blood Flow Metab. 36, 2162–2176. https://doi.org/10.1177/0271678X15614846

Stramaglia, Sebastiano, et al. "Synergetic and redundant information flow detected by unnormalized Granger causality: Application to resting state fMRI." *IEEE Transactions on Biomedical Engineering* 63.12 (2016): 2518-2524.

Takeuchi, N., Izumi, S.-I., 2012. Noninvasive Brain Stimulation for Motor Recovery after Stroke: Mechanisms and Future Views [WWW Document]. Stroke Res. Treat. https://doi.org/10.1155/2012/584727

Tang, C., Zhao, Z., Chen, C., Zheng, X., Sun, F., Zhang, X., Tian, J., Fan, M., Wu, Y., Jia, J., 2016. Decreased Functional Connectivity of Homotopic Brain Regions in Chronic Stroke Patients: A Resting State fMRI Study. PLoS ONE 11. https://doi.org/10.1371/journal.pone.0152875

Tang, Wei, et al. "Measuring Granger causality between cortical regions from voxelwise fMRI BOLD signals with LASSO." *PLoS Comput Biol* 8.5 (2012): e1002513.

Toga, A.W., Thompson, P.M., 2003. Mapping brain asymmetry. Nat. Rev. Neurosci. 4, 37–48. https://doi.org/10.1038/nrn1009

Treves, A., Panzeri, S., 1995. The Upward Bias in Measures of Information Derived from Limited Data Samples. Neural Comput. 7, 399–407. https://doi.org/10.1162/neco.1995.7.2.399

van der Knaap, L.J., van der Ham, I.J.M., 2011. How does the corpus callosum mediate interhemispheric transfer? A review. Behav. Brain Res. 223, 211–221.

https://doi.org/10.1016/j.bbr.2011.04.018

Yang, G.J., Murray, J.D., Repovs, G., Cole, M.W., Savic, A., Glasser, M.F., Pittenger, C., Krystal, J.H., Wang, X.-J., Pearlson, G.D., Glahn, D.C., Anticevic, A., 2014. Altered global brain signal in schizophrenia. Proc. Natl. Acad. Sci. 111, 7438–7443. https://doi.org/10.1073/pnas.1405289111